Molecular Biology of the Cell
Vol. 18, 3486–3501, September 2007

The *Trans*-Golgi Network Accessory Protein p56 Promotes Long-Range Movement of GGA/Clathrin-containing Transport Carriers and Lysosomal Enzyme Sorting [D] [V]

Gonzalo A. Mardones,*† Patricia V. Burgos,*† Doug A. Brooks,‡§ Emma Parkinson-Lawrence,‡§ Rafael Mattera,* and Juan S. Bonifacino*

*Cell Biology and Metabolism Branch, National Institute of Child Health and Human Development, National Institutes of Health, Bethesda, MD 20892; ‡Sansom Institute, University of South Australia, Adelaide, SA 5001, Australia; and §Lysosomal Diseases Research Unit, Department of Genetic Medicine, Children Youth and Women's Health Service, North Adelaide, SA 5006, Australia

Submitted March 1, 2007; Revised June 11, 2007; Accepted June 18, 2007
Monitoring Editor: Sandra Schmid

The sorting of acid hydrolase precursors at the *trans*-Golgi network (TGN) is mediated by binding to mannose 6-phosphate receptors (MPRs) and subsequent capture of the hydrolase-MPR complexes into clathrin-coated vesicles or transport carriers (TCs) destined for delivery to endosomes. This capture depends on the function of three monomeric clathrin adaptors named GGAs. The GGAs comprise a C-terminal "ear" domain that binds a specific set of accessory proteins. Herein we show that one of these accessory proteins, p56, colocalizes and physically interacts with the three GGAs at the TGN. Moreover, overexpression of the GGAs enhances the association of p56 with the TGN, and RNA interference (RNAi)-mediated depletion of the GGAs decreases the TGN association and total levels of p56. RNAi-mediated depletion of p56 or the GGAs causes various degrees of missorting of the precursor of the acid hydrolase, cathepsin D. In the case of p56 depletion, this missorting correlates with decreased mobility of GGA-containing TCs. Transfection with an RNAi-resistant p56 construct, but not with a p56 construct lacking the GGA-ear–interacting motif, restores the mobility of the TCs. We conclude that p56 tightly cooperates with the GGAs in the sorting of cathepsin D to lysosomes, probably by enabling the movement of GGA-containing TCs.

INTRODUCTION

The biosynthetic transport of acid hydrolases from the Golgi apparatus to the vacuole in yeast and to lysosomes in metazoans is a multistep process that is carried out by a complex molecular machinery. Genetic approaches have led to the identification and characterization of over 70 distinct vacuolar protein sorting or Vps proteins in the yeast, *Saccharomyces cerevisiae*, most of which are conserved in metazoans (Bowers and Stevens, 2005). The metazoan machinery is likely to comprise additional components that are needed to generate the greater diversity of lysosome structure, dynamics and function in multicellular organisms (Mullins and Bonifacino, 2001). However, only a few of the Vps homologues and additional components in metazoans have been directly demonstrated to participate in acid hydrolase sorting to lysosomes in vivo.

Among these are the transmembrane, cation-dependent (CD) and cation-independent (CI) mannose 6-phosphate receptors (MPRs) that sort newly synthesized lysosomal hydrolase precursors from the *trans*-Golgi network (TGN) to the endosomal-lysosomal system in mammals (Kornfeld, 1992; Ghosh *et al.*, 2003a). This sorting begins with the binding of the hydrolase precursors, via mannose 6-phosphate groups on their N-linked oligosaccharide chains, to the luminal domains of the MPRs. The cytosolic tails of the MPRs, in turn, interact with two types of clathrin adaptor, the monomeric GGA proteins (Puertollano *et al.*, 2001; Takatsu *et al.*, 2001; Zhu *et al.*, 2001) and the heterotetrameric AP1 complex (Höning *et al.*, 1997; Doray *et al.*, 2002; Ghosh and Kornfeld, 2004), leading to the concentration of the hydrolase-precursor–MPR complexes within clathrin-coated areas of the TGN (Klumperman *et al.*, 1993; Le Borgne and Hoflack, 1997). Clathrin-coated vesicles (CCVs) or pleiomorphic transport carriers (TCs) then form and deliver the hydrolase-precursor–MPR complexes to endosomes (Waguri *et al.*, 2002; Puertollano *et al.*, 2003; Polishchuck *et al.*, 2006). The hydrolase precursors subsequently dissociate from the MPRs and the former are carried to lysosomes with the fluid phase, where they become proteolytically processed to mature, active hydrolases. The unoccupied MPRs, on the other hand, return to the TGN to mediate further cycles of hydrolase precursor sorting.

The GGA proteins (i.e., GGA1, GGA2, and GGA3 in humans; Bonifacino, 2004; Ghosh and Kornfeld, 2004) are single-chain polypeptides comprising folded VHS, GAT, and GAE domains that are linked by largely unstructured segments. The link connecting the GAT and GAE domains is quite long and is referred to as "hinge." AP1 (Robinson, 2004; Owen *et al.*, 2004), on the other hand, is an oligomer,

This article was published online ahead of print in *MBC in Press* (http://www.molbiolcell.org/cgi/doi/10.1091/mbc.E07–02–0190) on June 27, 2007.

[D] [V] The online version of this article contains supplemental material at *MBC Online* (http://www.molbiolcell.org).

† These authors contributed equally to this work.

Address correspondence to: Juan S. Bonifacino (juan@helix.nih.gov).

comprising four subunits named β1, γ1, μ1, and σ1, the latter three of which occur as two or three isoforms. The N-terminal portions of β1 and γ1, plus the entire μ1 and σ1 subunits, assemble into a folded "core" domain, whereas the C-terminal portions of β1 and γ1 constitute largely unstructured "hinge" segments that end in globular "ear" domains. Despite their different quaternary structures, the GGAs and AP1 share some common structural and functional features. The VHS-GAT domains of the GGAs and the core domain of AP1, for example, participate in membrane recruitment and cargo recognition. The hinge domains of both types of adaptor bind clathrin. Finally the GAE domains of the GGAs and the ear domain of the γ1-adaptin subunit of AP1 (herein commonly referred to as GAE for gamma-adaptin ear) are structurally related and bind a common set of accessory proteins.

The GAE domains consist of an eight-stranded immunoglobulin-like β-sandwich (Nogi *et al.*, 2002; Collins *et al.*, 2003; Miller *et al.*, 2003). The surface of these domains share two shallow hydrophobic depressions that bind sequences conforming to the ΨG[PDE][ΨLM] motif (Ψ is an aromatic residue; pattern denoted according to PROSITE syntax; Mattera *et al.*, 2004) or related motifs (Kent *et al.*, 2002; Nogi *et al.*, 2002; Collins *et al.*, 2003; Miller *et al.*, 2003; Mattera *et al.*, 2003) on the accessory proteins. Among the proteins that are known to bind GAE domains through such motifs are rabaptin-5 (Hirst *et al.*, 2000; Doray and Kornfeld, 2001; Shiba *et al.*, 2002; Mattera *et al.*, 2003), γ-synergin (Page *et al.*, 1999; Hirst *et al.*, 2000; Takatsu *et al.*, 2000), NECAP1 and NECAP2 (Ritter *et al.*, 2003; Mattera *et al.*, 2004), aftiphilin (Mattera *et al.*, 2004), γ-BAR (Neubrand *et al.*, 2005), a protein known as Clint, enthoprotin, or epsinR (Kalthoff *et al.*, 2002; Wasiak *et al.*, 2002; Hirst *et al.*, 2003; Mills *et al.*, 2003), and p56 (Collins *et al.*, 2003; Lui *et al.*, 2003). The functions of these accessory proteins vis-à-vis their interactions with the GGAs and AP1 remain poorly understood.

Gene ablation and RNA interference (RNAi) approaches have been used to assess the requirement of the MPRs, the GGAs, AP1, and clathrin for the sorting of acid hydrolase precursors. Studies of MPR-deficient mice showed that both MPRs play partially redundant roles in this process (Koster *et al.*, 1993; Ludwig *et al.*, 1993; Ludwig *et al.*, 1996). The GGAs, however, appear to be nonredundant, because concurrent expression of all three human proteins is required for the sorting of cathepsin D to lysosomes, as shown by RNAi in HeLa cells (Ghosh *et al.*, 2003b). This nonredundancy has been attributed to the destabilization of the two remaining GGAs when any one of them is missing. Both gene deletion in mice and RNAi in cultured human cells have shown that AP1 is also required for acid hydrolase sorting (Meyer *et al.*, 2000; Hirst *et al.*, 2005). Paradoxically, ablation of the clathrin heavy-chain gene in chicken DT40 cells was shown not to affect acid hydrolase sorting (Wettey *et al.*, 2002), suggesting that clathrin might be dispensable for lysosomal sorting. This conclusion, however, conflicts with observations made using an antisense RNAi approach (Iversen *et al.*, 2003). The requirement of most GGA- and AP1-accessory proteins in acid hydrolase sorting remains to be assessed.

In this study, we have investigated the involvement of the accessory protein, p56, in lysosomal sorting. Extending previous studies (Lui *et al.*, 2003), we show that p56 colocalizes and interacts preferentially with the GGAs in vivo. p56 is, thus, the only TGN accessory protein described so far that displays specificity for the GGAs relative to AP1. Surprisingly, we find that depletion of any one GGA using synthetic siRNAs does not affect the levels or TGN localization of the other two GGAs. However, depletion of the GGAs does decrease the levels and TGN localization of p56. Depletion of p56, the GGAs or clathrin causes various degrees of missorting of the precursor form of the acid hydrolase, cathepsin D. In the case of p56 depletion, this missorting correlates with decreased mobility of GGA-containing TCs. Transfection with an RNAi-resistant p56 construct but not with a p56 construct lacking the GAE-interacting motif restores the mobility of the TCs. We conclude that p56 tightly cooperates with the GGAs and clathrin in the sorting of cathepsin D to lysosomes, probably by enabling the movement of GGA-containing TCs.

MATERIALS AND METHODS

Antibodies

The following mouse monoclonal antibodies were used: clone 8 to GGA3, clone 88 to γ1-adaptin, 9E10 to the Myc epitope, and clone 23 to the clathrin heavy chain (CHC; BD Biosciences, San Diego, CA); AC-40 to actin (Sigma-Aldrich, St. Louis, MO). The mouse monoclonal antibodies 6A1 to the VHS domain of human GGA1 and 4D2.5 to the hinge domain of human GGA2 were generated as previously described (Zola and Brooks, 1981) using purified GST-fusion proteins as immunogens. Positive clones were screened for reactivity to the GST-GGA fusion proteins by ELISA and assessed for specificity by screening for background reactivity with glutathione *S*-transferase (GST) protein. Hybridoma culture supernatants were purified on a 0.1-ml protein G cartridge (GE Healthcare, Rydalmere, NSW, Australia) and eluted with 0.1 M NaH_2PO_4, pH 2.5, into 100 μl of 1 M Na_2HPO_4, pH 9.0, and then dialyzed against three changes of phosphate-buffered saline (PBS). A polyclonal antibody to the hinge-GAE domains of GGA2 was raised in sheep. In addition, the following polyclonal antibodies were used: rabbit antibody to p56 raised against the N-terminal peptide, MDDDDFGGFEAAETFC, from human p56 (Covance Research Products, Denver, PA); rabbit antibody to GGA1 (gift of M. S. Robinson, University of Cambridge, United Kingdom); rabbit antibody to cathepsin D (cat # 219361; EMD Biosciences, La Jolla, CA); V-18 goat antibody to GAPDH (Santa Cruz Biotechnology, Santa Cruz, CA); sheep antibody to TGN46 (Serotec, Raleigh, NC); horseradish peroxidase–conjugated mouse anti-goat IgG (Pierce, Rockford, IL); horseradish peroxidase–conjugated donkey anti-mouse and donkey anti-rabbit IgG (Amersham Biosciences, Piscataway, NJ); Alexa-488– or -594–, or -647–conjugated donkey anti-mouse IgG, Alexa-488– or -594–conjugated donkey anti-rabbit IgG, and Alexa-488– or -594–, or -647–conjugated donkey anti-sheep IgG (Molecular Probes, Eugene, OR).

Recombinant DNA Procedures

For all p56 constructs, a cDNA encoding full-length isoform 1 of human p56 (GenBank/EMBL/DDBJ accession number NM_018318; Origene, Rockville, MD) was used as a template. Full-length p56 was obtained by PCR amplification and cloned in frame into the XhoI and SmaI sites of the pEYFP-C1 and pECFP-C1 (Cerulean variant) vectors (BD Biosciences Clontech, Palo Alto, CA; Rizzo *et al.*, 2004). Myc epitope-tagging at the N-terminus of p56 was performed through PCR amplification of the full-length p56 cDNA and cloning of this product in frame into the EcoRI and XbaI sites of the mammalian expression vector pCI-Myc_3 (Martina *et al.*, 2003). A construct lacking the N-terminal, GGA-interacting segment of p56 was cloned in frame into the EcoRI and XbaI sites of the pCI-Myc_3 vector (Myc-ΔN-p56; residues 125–441) using the same approach. The cloning of the Myc-epitope–tagged GGA1, Myc-epitope–tagged GGA3, and untagged GGA1 into pEYFP-C1 vector was described previously (Dell'Angelica *et al.*, 2000; Puertollano *et al.*, 2003). The nucleotide sequences of all these recombinant constructs were confirmed by dideoxy sequencing. To generate the cyan (Cerulean variant) fluorescent protein (CFP)-tagged GGA1 and AP1-γ1, untagged human GGA1 and γ1-adaptin subunit of AP1 (excised from an AP1-γ1-GFP construct provided by Lois Greene (National Heart, Lung, and Blood Institute, National Institutes of Health [NIH]; Wu *et al.*, 2003) were cloned in frame into the EcoRI and SalI, and XhoI and BamHI of pECFP-C2 and pECFP-N1 (BD Biosciences Clontech; Rizzo *et al.*, 2004), respectively.

Cell Culture and Transfections

HeLa (human epithelial), Jurkat (human T lymphoblast), SK-N-SH (human neuroblastoma), SK-N-MC (human neuroepithelioma), H4 (human neuroglioma), COS-7 (green monkey kidney fibroblast), and NRK (rat kidney fibroblast) cells were obtained from the American Type Culture Collection (Manassas, VA). Human fibroblasts in primary culture were kindly provided by C. L. Cadilla (Department of Biochemistry, University of Puerto Rico). M1 (human fibroblast), HEK-293 (human epithelial), and MNT-1 (human melanoma) cells were kindly provided by E. O. Long (National Institute of Allergy and Infectious Diseases, NIH), T. A. Rouault (National Institute of Child

Health and Human Development, NIH), and M. S. Marks (School of Medicine, University of Pennsylvania), respectively. HeLa, SK-N-SH, SK-N-MC, H4, COS-7, NRK, human fibroblasts in primary culture, M1, HEK-293, and MNT-1 cells were maintained in DMEM (Invitrogen, Carlsbad, CA). Jurkat cells were maintained in RPMI 1640 medium (Invitrogen). For all cell lines the media were supplemented with 2 mM glutamine, 100 U/ml penicillin, 100 μg/ml streptomycin, and 10% (vol/vol) fetal bovine serum (FBS; Invitrogen), except for MNT-1 for which it was supplemented with 20% (vol/vol) FBS (Hyclone, Logan, UT) and 10% AIM-V medium (Invitrogen). Human fibroblasts in primary culture, SK-N-SH, SK-N-MC and MNT-1 media were also supplemented with 0.1 mM nonessential amino acids (Invitrogen). Transfections were carried out using the Lipofectamine 2000 reagent (Invitrogen) according to the manufacturer's instructions. The cells were analyzed 16–24 h after transfection, with the exception of cells transfected with AP1-γ1-CFP, which were analyzed after 48 h of expression.

Immunofluorescence Microscopy, Quantitative Analysis, and Förster Resonance Energy Transfer Imaging

Indirect immunofluorescence staining of fixed, permeabilized cells was performed as described previously (Mardones *et al.*, 2006). Images of either fixed or live transfected cells were acquired with an Olympus FluoView FV1000 scanning unit fitted on an inverted Olympus IX81 microscope, used with a PlanApo 60× oil immersion objective (NA 1.40; Olympus, Melville, NY). Analysis of colocalization by immunofluorescence microscopy was performed after correction for noise, cross-talk, and background signals on each set of images. For each pairwise comparison we obtained three values, M_1, M_2, and r, according to Manders *et al.* (1992). M_1 is defined as the ratio: (summed intensities of pixels from channel-A for which the intensity in channel-B is above zero):(total intensity in channel-A), and M_2 is the converse ratio. M_1 and M_2 vary from 0 to 1, corresponding to no colocalization and complete colocalization, respectively. To evaluate quantitatively the level of colocalization, the Pearson's correlation coefficient, r (Manders *et al.*, 1992) was also calculated, with one indicating complete positive correlation and zero indicating no correlation. All values were obtained with the plug-in JACoP (Bolte and Cordelières, 2006; http://rsb.info.nih.gov/ij/plugins/track/jacop.html), developed for the image analysis software ImageJ 1.36b (Rasband, 1997, 2007). Each pairwise comparison was done on five sets of images acquired with the same optical settings, and the mean and SD of each parameter are presented in Supplementary Table 1. For Förster resonance energy transfer (FRET) imaging, NRK cells grown in 35-mm glass-bottom culture dishes (MatTek, Ashland, MA) were maintained in phenol red–free buffered medium and held at 37°C with an ASI 400 Air Stream stage Incubator (Nevtek, Burnsville, VA). Sensitized emission FRET analysis was quantified with the three built-in filter settings for the CFP, yellow fluorescent protein (YFP), and CFP/YFP/FRET channels. The excitation light sources were a 30-mW multiline Argon laser (457, 488, and 515 nm), a 25-mW 405-nm laser diode, and a 5.3-mW 440-nm laser diode, each at 2.0% intensity. Image capture and data acquisition were performed using Olympus FV1000 application software (FV10-ASW). The images were acquired at 250 dpi. Background subtraction was made before the FRET calculations. For correction of cross-talk between CFP and YFP channels, constructs encoding CFP- or YFP-fusion proteins were expressed separately, and for each fluorophore the emission from the FRET channel was divided by the emission measured in either the CFP or YFP channels. Corrected FRET was calculated on a pixel-by-pixel basis as described (Gordon *et al.*, 1998), and the FRET-corrected images were displayed in pseudocolor mode.

RNAi

RNAi was performed using siRNAs (Dharmacon, Lafayette, CO) designed to the following human target sequences: AAUGCUCAGCAUCAGAGGCUC for the coding sequence of p56, AAGAAUGGAUUGAUGAU for the 5′ untranslated region of p56 (p56-5′), CAUCGUGUUCCAGUCAGCU for GGA1, UACACCUCUGGCUCAAGUG for GGA2, CAGUUUGUCCUCCGUGUUGG for GGA3, and UCCAAUUCGAAGACCAAUU for CHC. For the design of the siRNAs to the GGAs, an alignment of the cDNAs of the human sequences (Accession numbers: NM_013365 for GGA1; NM_015044 for GGA2; and NM_014001 for GGA3), using the multiple sequence alignment algorithm ClustalW (Thompson *et al.*, 1994), was performed. We selected 18–20-base oligonucleotides directed to regions in the aligned coding sequences with the lowest degree of identity among the GGAs. Oligonucleotides with the ability to produce a knockdown of ≥90%, as assessed by immunoblot analysis, were chosen for further experiments. RNAi for human γ1-adaptin was performed with siGENOME Smart Pool siRNAs (Dharmacon). RNAi for GAPDH was performed with a siControl duplex siRNA (Dharmacon). Cells were transfected with the siRNAs using Oligofectamine (Invitrogen) according to the manufacturer's protocol. For knockdown of the GGAs, cells were transfected twice at 72-h intervals and analyzed 72 h after the second round of transfection. For knockdown of GAPDH, p56, γ1-adaptin, and CHC cells were transfected twice at 24-h intervals and analyzed 48 h after the second round of transfection.

Electrophoresis and Immunoblotting

SDS-PAGE analysis and electroblotting onto nitrocellulose membranes were performed using the NuPAGE Bis-Tris Gel system (Invitrogen), according to the manufacturer's instructions. Incubations of the nitrocellulose membranes with primary and secondary antibodies were performed as previously described (Burgos *et al.*, 2004). Horseradish peroxidase–labeled antibodies were detected using electrochemiluminescence (ECL) Western Blotting Substrate from Pierce (Rockford, IL).

Metabolic Labeling and Immunoprecipitation

Metabolic labeling of cells was carried out as described (Kametaka *et al.*, 2007). Briefly, cells grown on six-well plates were pulse-labeled for 2 h at 20°C using 0.1 mCi/ml [^{35}S]methionine-cysteine (Express Protein Label; Perkin Elmer-Cetus Life and Analytical Sciences, Boston, MA) and chased for 1–5 h at 37°C in regular culture medium in the presence of 5 mM mannose 6-phosphate, 0.06 mg/ml methionine and 0.1 mg/ml cysteine. After chase, cells were rinsed twice with PBS and subjected to lysis in 50 mM Tris, pH 7.5, 150 mM NaCl, 10% glycerol, 5 mM EDTA, 1% (vol/vol) Triton X-100, and a complete protease inhibitor cocktail (Roche Applied Science, Indianapolis, IN). The extracts were immunoprecipitated and analyzed by SDS-PAGE and fluorography. Quantification was performed on a Typhoon 9200 PhosphorImager (Amersham Biosciences) using ImageQuant analysis software.

Time-Lapse Microscopy and Image Analysis

Mock- or p56-depleted, live H4 cells were transfected with YFP-GGA1, plated on 35-mm glass-bottom culture dishes (MatTek), and maintained in phenol red–free buffered medium at 37°C by using an ASI 400 Air Stream stage Incubator (Nevtek, Burnsville, VA). Time-lapse fluorescence images were acquired with an Ultraview Confocal Scanner (Perkin Elmer-Cetus, Norwalk, CT) in a Nikon Eclipse TE2000-S inverted microscope (Nikon, Melville, NY) equipped with a PlanApo 100× oil immersion objective (NA 1.40; Nikon), and a 12-bit charge-coupled device (CCD) camera, ORCA (Hamamatsu, Bridgewater, NJ). Image capture and data acquisition were performed using Ultraview LCI software (Perkin Elmer-Cetus). Images were acquired in binning 2 × 2 modes to increase the signal to noise ratio, at ~0.25-s intervals, during 110–120 s. Sequence images were exported as single TIFF files, and processed with MetaMorph (Molecular Devices, Sunnyvale, CA), and ImageJ 1.36b (Rasband, 1997, 2007; http://rsb.info.nih.gov/ij/). Vesicles were counted and movement was tracked manually with an especially developed plug-in for ImageJ (http://rsb.info.nih.gov/ij/plugins/track/track.html, Fabrice P. Cordelières, Institut Curie, France). The distance reached by vesicles was determined by measuring the movement between successive frames. Each experiment was repeated at least 15 times under identical conditions, and the mean and SD for each parameter were calculated. To prepare figures, single frames were processed with Adobe Photoshop 7 (Adobe Systems, Mountain View, CA). QuickTime movies were produced using ImageJ 1.36b.

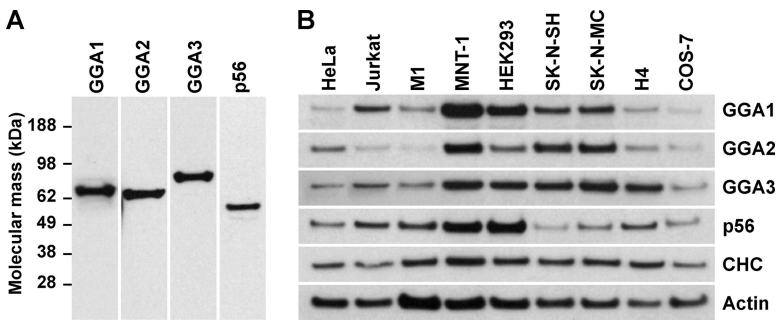

Figure 1. Expression of GGAs and p56 in different cell lines. (A) Detection of endogenous GGA1, GGA2, GGA3, and p56 in HeLa cells by immunoblot analysis using specific mouse monoclonal antibodies to each GGA and a rabbit polyclonal antibody to p56. The positions of molecular mass markers are indicated on the left. (B) Immunoblot analysis of the expression of the proteins indicated on the right in the different cell lines indicated on top.

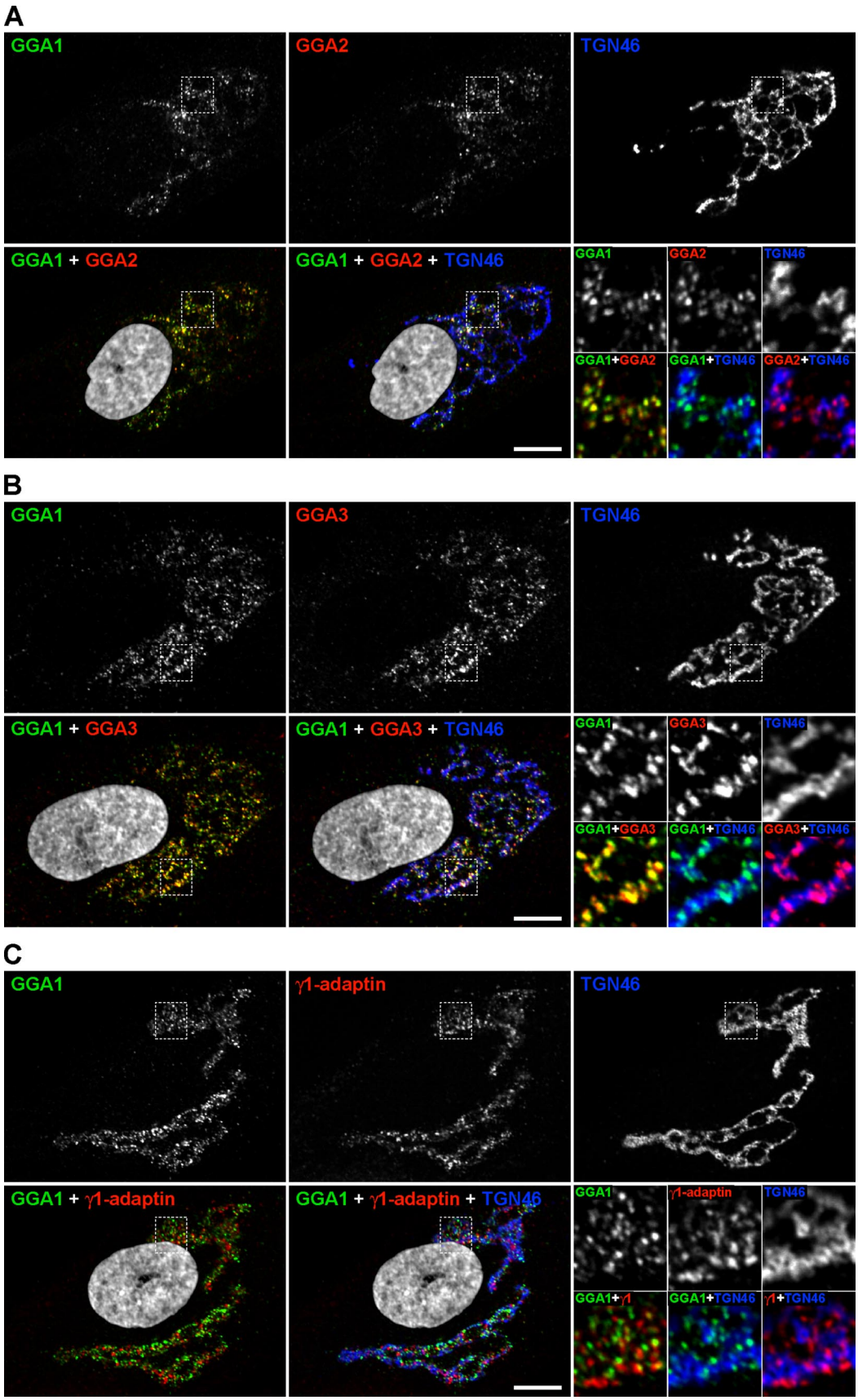

Figure 2. Comparison of the intracellular localization of endogenous GGAs and AP1 by confocal immunofluorescence microscopy. Human fibroblasts grown on coverslips were fixed, permeabilized, and triple-labeled with rabbit polyclonal antibody to GGA1 (A–C), mouse

RESULTS

Ubiquitous Expression of the GGAs and p56 in Human Cell Lines

As a first step to investigate the possible functional cooperation of the GGAs and p56, we examined the pattern of expression of these proteins in nine different human cell lines. These analyses were made possible by the recent development of a complete panel of antibodies that detect the endogenous GGAs and p56 by immunoblotting and immunofluorescence microscopy. We observed that the three human GGAs were expressed in all cell lines tested, regardless of their lineage (Figure 1). The ratios of the three GGAs, however, varied among the different cell lines, with GGA1 being relatively more abundant in Jurkat (T-cell), MNT-1 (melanocyte), and HEK293 (epithelial), GGA2 in HeLa (epithelial), and GGA3 in H4 (neuroglioma) cells (Figure 1). Likewise, p56 was expressed in all the tested cell lines, being more abundant in MNT-1 and HEK293 cells (Figure 1). Similar results were obtained by immunofluorescence microscopy (data not shown). These observations are in accordance with the results of Northern analyses of GGA mRNA expression (Boman *et al.*, 2000; Dell'Angelica *et al.*, 2000; Poussu *et al.*, 2000) and indicate that the three GGA proteins as well as p56 are ubiquitously expressed.

Colocalization of Endogenous GGAs and p56 to the TGN

The availability of a set of antibodies that detect the endogenous GGAs also allowed us to compare their localizations within cells. Previous comparative analyses of localization were carried out mostly by transfection of tagged GGA constructs (Boman *et al.*, 2000; Dell'Angelica *et al.*, 2000; Hirst *et al.*, 2000; Ghosh *et al.*, 2003b) and were therefore liable to overexpression problems. To optimize the resolution of intracellular structures, we performed immunofluorescence microscopy on human fibroblasts in primary culture, which are unusually large and flat cells. Quadruple staining of these cells for combinations of two GGAs, the TGN marker TGN46, and nuclear DNA, showed that the three GGAs colocalized to the same set of juxtanuclear puncta aligned with the TGN (>80% colocalization, $r = \sim 0.90$; Figure 2, A and B, and Supplementary Table 1). Using a similar procedure, we observed that the γ1-adaptin subunit of AP1 localized to a largely distinct set of puncta that did not stain for GGA1 (~9% colocalization, $r = \sim 0.12$; Figure 2C and Supplementary Table 1) or the other GGAs (data not shown). Finally, we found that p56 also localized to TGN puncta that coincided more with GGA3 (>70% colocalization, $r = \sim 0.84$; Figure 3A and Supplementary Table 1) and the other GGAs (data not shown) than with AP1-γ1 (~11% colocalization, $r = \sim 0.19$; Figure 3B and Supplementary Table 1). We also observed considerable colocalization of p56 with clathrin (~50% of p56, $r = \sim 0.43$; Figure 3C and Supplementary Table 1). These observations point to the existence of at least two types of clathrin-coated structure in association with the TGN, which are defined by the presence of GGA/p56 and AP1, respectively. These two types could correspond to functionally distinct populations of clathrin-coated structures or to different stages of maturation of the same population, as predicted by the GGA-to-AP1 transfer model of MPR sorting at the TGN (Doray *et al.*, 2002). The three GGAs and p56 were also found to colocalize to faint peripheral cytoplasmic foci that likely correspond to TCs and endosomes (data not shown), as previously shown for epitope- and GFP-tagged GGAs (Puertollano *et al.*, 2003; Puertollano and Bonifacino, 2004; Wahle *et al.*, 2005; Polishchuk *et al.*, 2006).

In Vivo Interactions of the GGAs with p56 Detected by FRET

The immunofluorescence microscopy analyses described above (Figures 2 and 3; see also Lui *et al.*, 2003), in conjunction with previous in vitro binding studies (Collins *et al.*, 2003; Lui *et al.*, 2003), suggested that p56 might physically interact with the GGAs at the TGN. To test whether this was the case in vivo, we performed FRET imaging. This technique can detect the physical proximity of two different fluorophores on a scale of ångströms (<80 Å; Gordon *et al.*, 1998) and has been successfully used to demonstrate physical association and oligomerization of many proteins in live cells (see for example Galperin and Sorkin, 2003). To this end, CFP-tagged GGA1 and YFP-tagged p56 were coexpressed by transient transfection in NRK cells (to get low levels of expression). We observed that these constructs yielded a strong FRET signal at the TGN (n = 12; Figure 4A). Similar observations were made for CFP-p56 and YFP-GGA1 (n = 11), and for CFP-GGA3 and YFP-p56 (n = 12) (data not shown). Using the same experimental protocol, we found that CFP-p56 and YFP-p56 also exhibited FRET at the TGN (n = 15; Figure 4A), consistent with the dimerization of p56 inferred from in vitro cross-linking experiments (Lui *et al.*, 2003). Importantly, although both AP1-γ1-CFP and YFP-p56 exhibited TGN localization, they showed no significant FRET (n = 8; Figure 4A), thus verifying the specificity of the other FRET signals. From these experiments, we concluded that GGA1 and GGA3, but not AP1-γ1, interact with p56 dimers at the TGN in vivo.

TGN Localization and Total Levels of p56 Are Dependent on the GGAs

We next sought to assess the interdependence of the localization and levels of the GGAs and p56 in cells. We observed that moderate overexpression of Myc-epitope–tagged GGA1 (Myc-GGA1) in NRK cells markedly increased the TGN staining, while decreasing the cytosolic staining of endogenous p56 (Figure 4B). Similar observations were made for Myc-epitope–tagged GGA2 and GGA3 (data not shown). The converse was not the case, as moderate overexpression of Myc-epitope–tagged p56 did not alter the distribution of the endogenous GGAs (data not shown). These observations provided further evidence for the interaction of the GGAs with p56 in vivo and indicated that the GGAs promote the recruitment of p56 to the TGN but not the other way around.

Figure 2 (cont). monoclonal antibodies to GGA2 (A), GGA3 (B), or the γ1-adaptin subunit of AP1 (C), and sheep antibody to TGN46 (A–C), followed by Alexa-488–conjugated donkey anti-rabbit IgG (green channel), Alexa-594–conjugated donkey anti-mouse IgG (red channel), and Alexa-647–conjugated donkey anti-sheep IgG (blue channel). Nuclei were stained with Hoechst 33342 dye (gray channel). Stained cells were examined by confocal fluorescence microscopy. Merging of the images in the green, red, and gray channels generated the first picture in the second row; yellow indicates overlapping localization of the green and red channels. The second picture in the second row was generated by merging of the images in the green, red, blue, and gray channels; yellow indicates overlapping localization of the green and red channels, cyan indicates overlapping localization of the green and blue channels, magenta indicates overlapping localization of the red and blue channels, and white indicates overlapping localization of the red, green, and blue channels. The third panel in the second row is a composite of threefold magnified views of the Golgi region marked with a dashed box in the indicated channels. Bars, 10 μm.

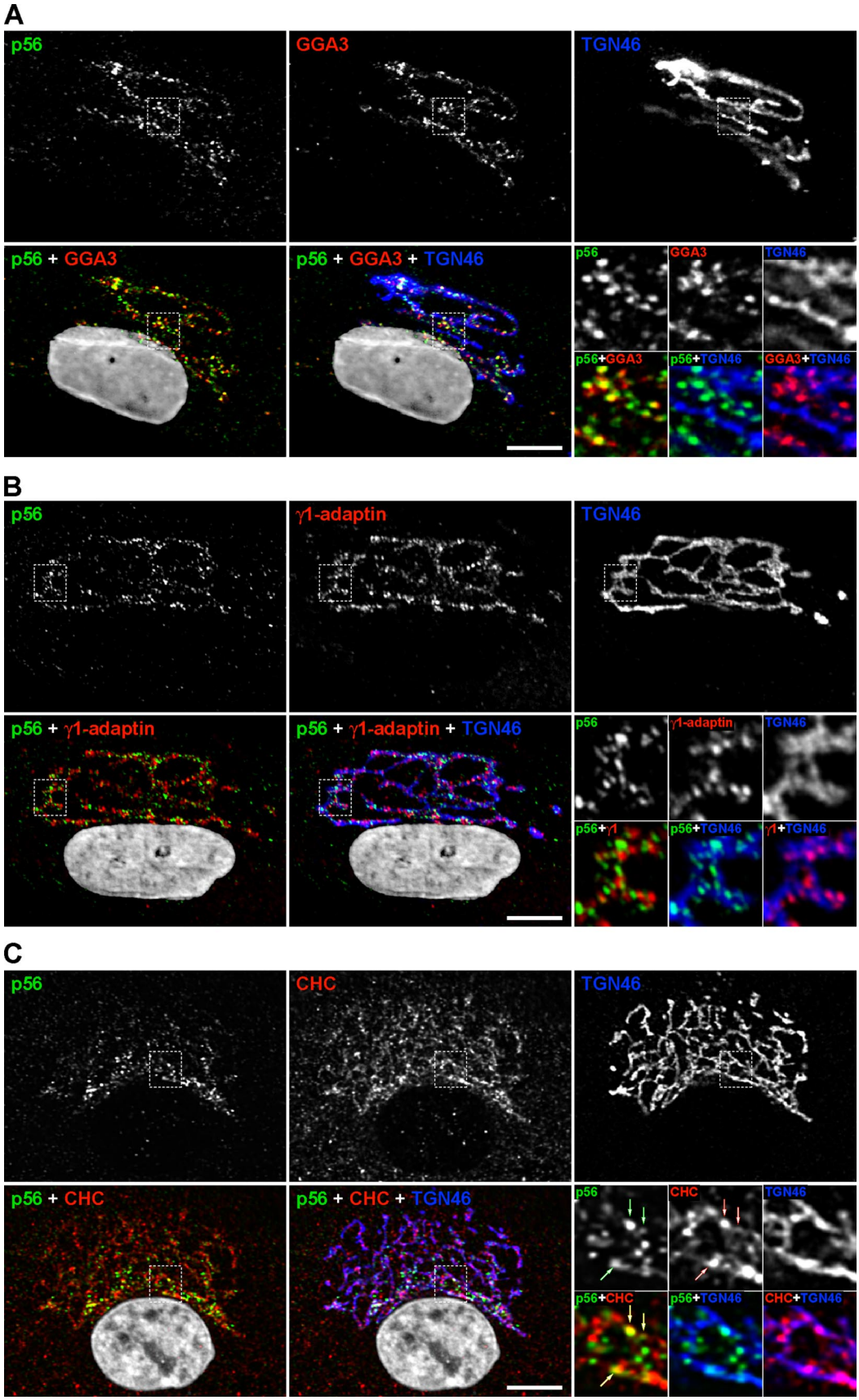

Figure 3. Comparison of the intracellular localization of endogenous p56, GGA3, AP1, and clathrin analyzed by confocal immunofluorescence microscopy. Human fibroblasts grown on coverslips were fixed, permeabilized, and triple-labeled with rabbit polyclonal antibody to

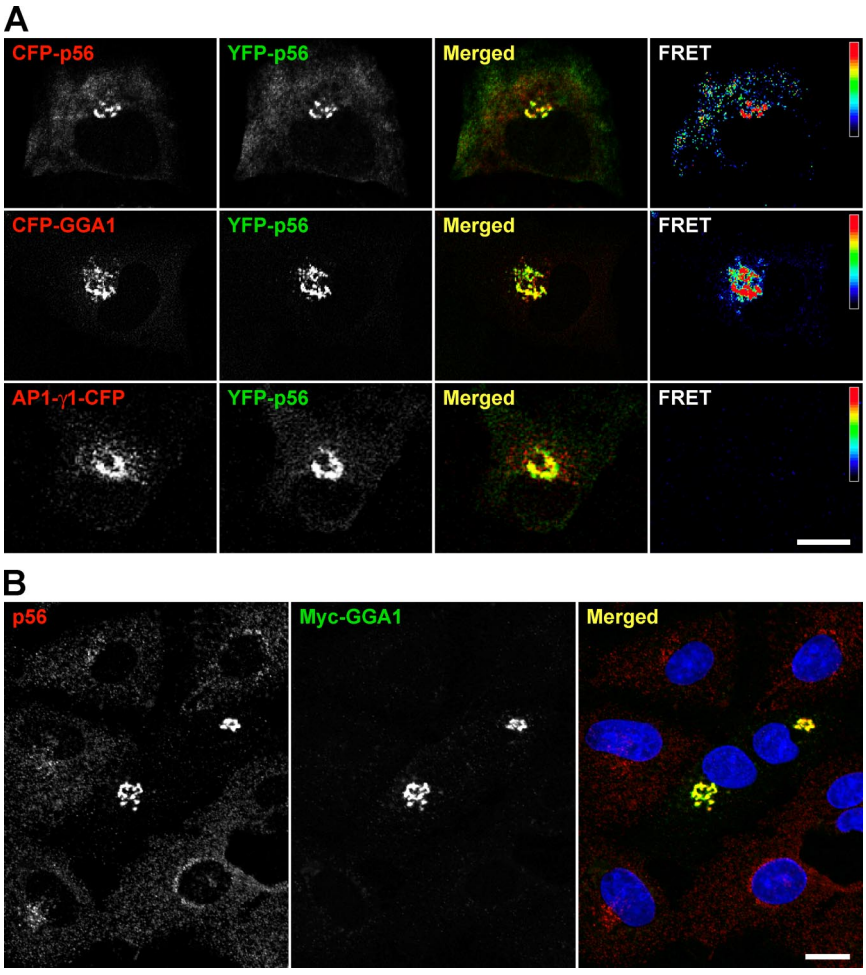

Figure 4. Interactions of p56 and GGAs demonstrated by FRET analysis and corecruitment to the TGN. (A) Live NRK cells expressing the indicated CFP- (red channel) and YFP-fusion (green channel) proteins were imaged at 37°C by confocal fluorescence microscopy. FRET signals were acquired immediately after recording of the signals in the red and green channels. Merging red and green channels generated the third picture in each row. The fourth picture in each row represents a FRET-corrected image displayed in pseudocolor mode, with red and blue areas corresponding to high and low FRET values, respectively. (B) NRK cells transfected with Myc-tagged GGA1 were fixed, permeabilized, and double-labeled with rabbit polyclonal antibody to p56 and mouse mAb to the Myc epitope, followed by Alexa-594–conjugated donkey anti-rabbit IgG (red channel) and Alexa-488–conjugated donkey anti-mouse IgG (green channel). Nuclei were stained with Hoechst 33342 dye (blue channel). Stained cells were examined by confocal fluorescence microscopy. Merging red, green, and blue channels generated the third picture; yellow indicates overlapping localization of the green and red signals. Bars, 10 μm.

To further investigate this interdependence, we used synthetic, small interfering RNAs (siRNAs) to deplete the GGAs and p56, as well as glyceraldehyde-3-phosphate dehydrogenase (GAPDH; Mock), γ1-adaptin, or CHC, in HeLa cells. The siRNAs targeting each GGA were designed to maximize the number of mismatches relative to the other two GGAs (see *Materials and Methods*), thus decreasing the probability of "cross-depletion." The levels of all the target proteins could be reduced greater than 90% by this procedure, as detected by immunoblot analysis (Figure 5). We observed

Figure 3 (cont). p56 (A–C), mouse monoclonal antibodies to GGA3 (A), the γ1-adaptin subunit of AP1 (B), or clathrin heavy chain (C), and sheep antibody to TGN46 (A–C), followed by Alexa-488–conjugated donkey anti-rabbit IgG (green channel), Alexa-594–conjugated donkey anti-mouse IgG (red channel), and Alexa-647–conjugated donkey anti-sheep IgG (blue channel). Nuclei were stained with Hoechst 33342 dye (gray channel). Stained cells were examined by confocal fluorescence microscopy. Merging of the images in the green, red, and gray channels generated the first picture in the second row; yellow indicates overlapping localization of the green and red channels. Merging of the images in the green, red, blue, and gray channels generated the second picture in the second row; yellow indicates overlapping localization of the green and red channels, cyan indicates overlapping localization of the green and blue channels, magenta indicates overlapping localization of the red and blue channels, and white indicates overlapping localization of the red, green, and blue channels. The third panel in the second row is a composite of threefold magnified views of the Golgi region marked with a dashed box in the indicated channels. Arrows in C point to foci of colocalization. Bars, 10 μm.

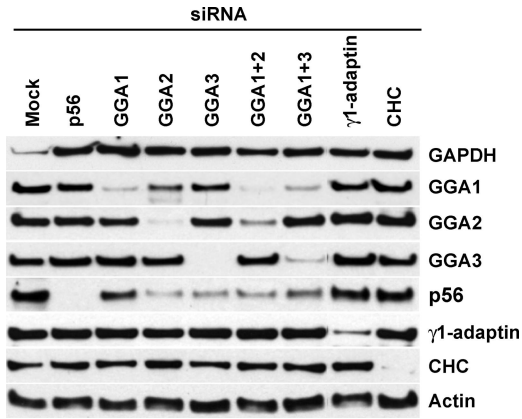

Figure 5. Biogenetic relationships of the GGAs and p56 examined by RNAi-mediated depletion. HeLa cells were transfected twice with siRNAs directed to GAPDH (Mock), p56, GGA1, GGA2, GGA3, GGA1 plus GGA2 (GGA1 + 2), GGA1 plus GGA3 (GGA1 + 3), the γ1-adaptin subunit of AP1, or CHC. After the second round of transfection, equivalent amounts of homogenates of siRNA-treated cells were subjected to SDS-PAGE and immunoblotting using antibodies to the proteins indicated on the right.

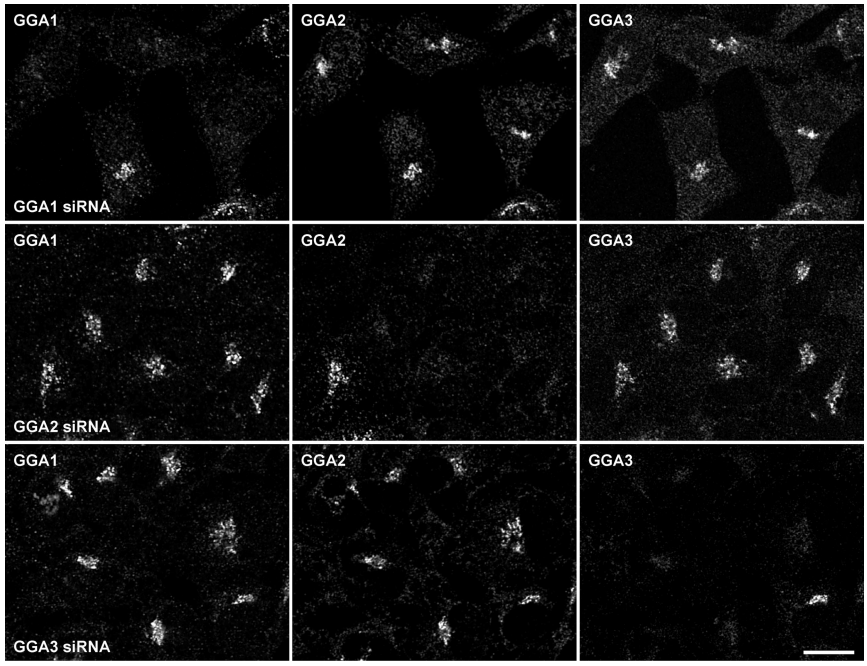

Figure 6. Effects of the depletion of individual GGAs on the intracellular localization of the remaining GGAs. The effects of depletion of GGA1 (first row), GGA2 (second row), or GGA3 (third row) on the expression and distribution of the remaining GGAs in HeLa cells were assessed by indirect immunofluorescence microscopy. Mixed mock- and siRNA-treated cells grown on coverslips were fixed, permeabilized, and triple-labeled with rabbit polyclonal antibody to GGA1, sheep polyclonal antibody to GGA2, and mouse mAb to GGA3, followed by Alexa-594–conjugated donkey anti-rabbit IgG (red channel), Alexa-488–conjugated donkey anti-sheep IgG (green channel), and Alexa-647–conjugated donkey anti-mouse IgG (blue channel). Stained cells were examined by confocal fluorescence microscopy. Bar, 10 μm.

that individual depletion of each GGA had no effect on the levels of the other two GGAs (Figure 5; the decreased level of GGA1 in the GGA2-depleted cells seen in Figure 5 was not reproducible; see an example of another experiment in Supplementary Figure 1). In addition, we could achieve good, albeit less complete, depletion of combinations of

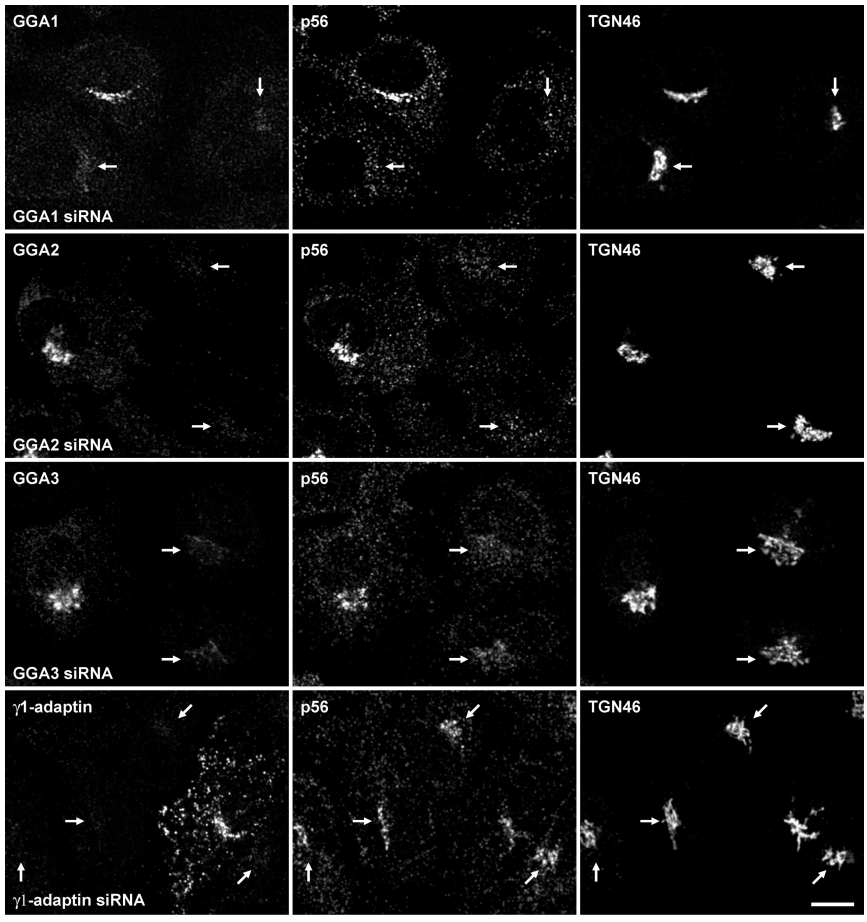

Figure 7. Effect of the depletion of GGAs on the intracellular localization of p56. HeLa cells were transfected twice with siRNAs directed to GAPDH (Mock), GGA1, GGA2, GGA3, or the γ1-adaptin subunit of AP1, as indicated in the figure. After the second round of transfection, the effects of the RNAi depletion on the distribution of p56 in cells were assessed by confocal immunofluorescence microscopy. Mixed mock- and siRNA-treated cells grown on coverslips were fixed, permeabilized, and triple-labeled with mouse monoclonal antibodies to GGA1 (first row), GGA2 (second row), GGA3 (third row), or the γ1-adaptin subunit of AP1 (fourth row), rabbit polyclonal antibody to p56, and sheep polyclonal antibody to TGN46, followed by Alexa-594–conjugated donkey anti-mouse IgG (red channel), Alexa-488–conjugated donkey anti-rabbit IgG (green channel), and Alexa-647–conjugated donkey anti-sheep IgG (blue channel). Stained cells were examined by confocal fluorescence microscopy. Arrows indicate the position of the Golgi complex in siRNA-depleted cells. Bar, 10 μm.

GGA1+GGA2 or GGA1+GGA3 without affecting the levels of the remaining GGA (Figure 5). Similar observations were made by immunofluorescence microscopy, in which depletion of each GGA did not affect the intensity of TGN staining of the other two (Figure 6). Thus, each GGA behaves as a biogenetically independent species, such that the absence of one does not alter the level or localization of the others.

Strikingly, depletion of any one GGA caused a partial decrease in the levels of endogenous p56 detected by immunoblotting (Figure 5) and its staining at the TGN observed by immunofluorescence microscopy (Figure 7). These effects were specific, as depletion of GAPDH, γ1-adaptin and CHC had no effect on p56 levels (Figure 5) and TGN localization (Figure 7 and data not shown). Biochemical analyses showed that, although decreasing the total levels of p56, GGA depletion did not affect the ratio of membrane-bound to cytosolic p56 (data not shown). The decrease in the level of p56 associated to the TGN could be reverted by moderate overexpression of any one GGA, as exemplified in Figure 8 for GGA2-depleted cells expressing Myc-epitope–tagged GGA3. From these experiments we concluded that p56 depends on the total levels of GGAs, but not AP1, for its stability and localization to the TGN.

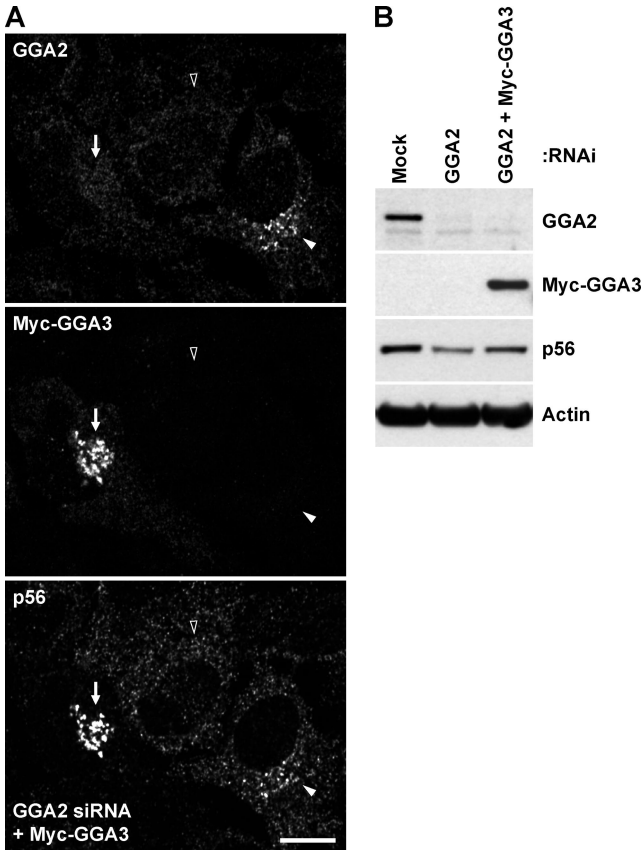

Figure 8. Effect of moderate overexpression of Myc-GGA3 on p56 levels in cells depleted of GGA2. (A) HeLa cells were transfected twice with siRNAs directed to GAPDH (Mock), or GGA2. After the second round of siRNA treatment, GGA2-depleted cells were transfected with Myc-GGA3, and after 16 h, the effects of Myc-GGA3 on the distribution of p56 in cells were assessed by indirect immunofluorescence. Mixed mock- and GGA2-depleted cells grown on coverslips were fixed, permeabilized, and triple-labeled with sheep antibody to GGA2, mouse antibody to the Myc epitope, and rabbit antibody to p56, followed by Alexa-594–conjugated donkey anti-sheep IgG (red channel), Alexa-488–conjugated donkey anti-mouse IgG (green channel), and Alexa-647–conjugated donkey anti-rabbit IgG (blue channel). Solid arrowheads indicate the position of the Golgi complex in a mock-depleted, untransfected cell. Open arrowheads indicate the position of the Golgi complex in a GGA2-depleted, untransfected cell. Arrows indicate the position of the Golgi complex in a GGA2-depleted, Myc-GGA3–expressing cell. Bar, 10 μm. (B) Equivalent amounts of HeLa cells transfected with siRNAs and Myc-GGA3 as indicated in A, were subjected to SDS-PAGE and immunoblotting using antibodies to GGA2, the Myc epitope, p56, or actin (loading control).

Depletion of p56 Impairs the Sorting of Cathepsin D

The GGAs participate in the sorting of MPRs between the TGN and endosomes, thus enabling the transport of newly synthesized acid hydrolase precursors to lysosomes (Puertollano *et al.*, 2001; Zhu *et al.*, 2001; Ghosh *et al.*, 2003b). The close physical and biogenetic relationship of p56 to the GGAs raised the possibility that p56 might likewise be involved in lysosomal sorting. To determine if this was the case, we examined the effect of depleting cells of p56 on the proteolytic maturation of the precursor of the acid hydrolase, cathepsin D, which takes place upon transport to lysosomes. In control cells, the 53-kDa precursor form is first cleaved to a 47-kDa intermediate form and, subsequently, to 31-kDa heavy-chain and 15-kDa light-chain mature forms. Immunoblot analysis of HeLa cell extracts showed that, at steady state, most of the cathepsin D occurred as the 31-kDa mature heavy chain (the 15-kDa light chain was not detected by the antibody), with only minute amounts of the precursor and intermediate forms (Figure 9A). RNAi-mediated depletion of p56, as well as of GGA1, GGA2, GGA3, γ1-adaptin, or CHC, increased the steady-state levels of the cathepsin D precursor by ~4- to ~6-fold (Figure 9, A and B). Depletion of GGA2 and γ1-adaptin also resulted in increased levels of the intermediate form (Figure 9A). The higher levels of immature cathepsin D forms in cells depleted of any of the above proteins were indicative of impaired transport of the enzyme to lysosomes.

To further examine the involvement of p56 and related proteins in the lysosomal sorting of cathepsin D, we performed pulse-chase analyses. RNAi-treated HeLa cells were metabolically labeled with [^{35}S]methionine-cysteine for 2 h at 20°C (to arrest transport at the TGN) and then chased in complete medium for different periods at 37°C. Cathepsin D species were isolated by immunoprecipitation and resolved by SDS-PAGE and fluorography. Using this protocol, we could follow the kinetics of cathepsin D processing in cells depleted of different proteins. In control cells, the precursor form was cleaved to the intermediate form and then to the 31-kDa mature form over a 5-h period (Figure 9, C and D; the 15-kDa mature light chain has a low content of methionine and cysteine and was therefore not well labeled in these experiments). Quantification of these results showed that at 3 h of chase the precursor form accounted for ~35% and the mature form ~40% of the total labeled cathepsin D. At 5 h these values were ~15% for the precursor form and ~65% for the mature form. Depletion of p56 caused a significant delay in the processing of cathepsin D, such that at 3 h of chase ~65% corresponded to the precursor form and ~12% to the mature form (Figure 9, C and D). The delay was also manifest at 5 h of chase, when ~35% remained as the precursor form and only ~40% was processed to the mature form. These numbers were indicative of a ~2-h delay in the overall kinetics of processing. Depletion of each of the GGAs, γ1-adaptin, or CHC all delayed cathepsin D maturation, albeit to different extents, with GGA3 depletion having a relatively minor effect and CHC depletion the strongest effect (Figure 9, C and D). Taken together, these experiments

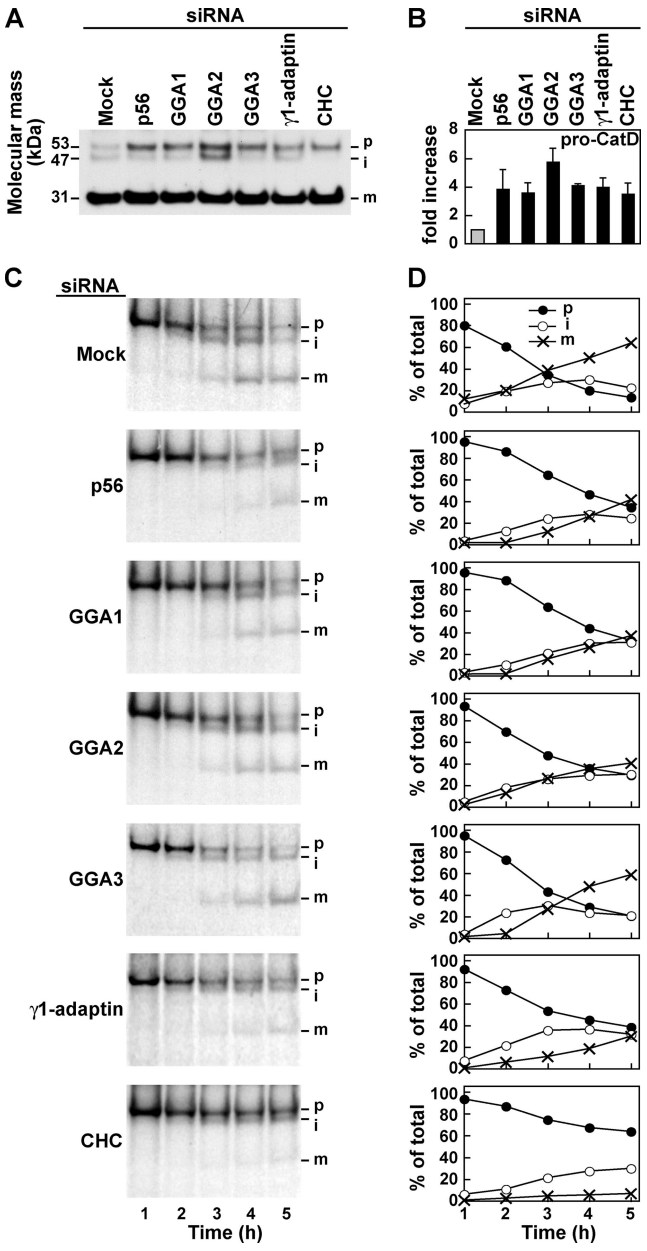

Figure 9. Immunoblot and pulse-chase analysis of the maturation of cathepsin D in cells depleted of GGAs or p56. (A) HeLa cells were transfected twice with siRNAs directed to GAPDH (Mock), p56, GGA1, GGA2, GGA3, the γ1-adaptin subunit of AP1, or CHC. After the second round of transfection, equivalent amounts of homogenates of siRNA-treated cells were subjected to SDS-PAGE and immunoblotting using antibody to cathepsin D. The positions and molecular masses (in kDa) of marker proteins are indicated on the left. (B) The densities of the immunoblot signals for the precursor form of cathepsin D from A were determined, and the fold increase for each RNAi treatment was calculated. Bars represent the mean ± SD from three independent experiments. (C) HeLa cells were transfected twice with siRNAs directed to GAPDH (Mock), p56, GGA1, GGA2, GGA3, the γ1-adaptin subunit of AP1 or CHC. After the second round of transfection, cells were metabolically labeled for 2 h at 20°C with [^{35}S]methionine-cysteine and chased for different periods at 37°C. Cells were solubilized, and the extracts were subjected to immunoprecipitation of cathepsin D. The immunoprecipitates were analyzed by SDS-PAGE and fluorography. (A and C) The positions of the precursor (p), intermediate (i), and mature heavy chain (m) forms of cathepsin D are indicated on the right. (D) The autoradiographic density of each cathepsin D species from C was determined, and the percentage of each form at each chase time was calculated after normalization for the number of methionine and cysteine residues.

demonstrated that, like the GGAs, AP1, and clathrin, p56 is involved in the sorting of cathepsin D to lysosomes.

Depletion of p56 Decreases the Mobility of GGA-containing Carriers

To determine whether the slower kinetics of cathepsin D processing in p56-depleted cells were due to alteration of the localization of other components of the lysosomal sorting machinery, we performed immunofluorescence microscopy. We found that depletion of p56 did not cause any obvious change in the steady-state distribution of the GGAs (shown for GGA1 in Figure 10A), AP1, clathrin, CI-MPR, and CD-MPR (data not shown). Likewise, we did not see any effect of p56 depletion on the overall appearance of the Golgi complex, as detected by staining for the TGN marker, TGN46 (Figure 10A), and the *cis*-Golgi marker, GM130 (data not shown).

To assess whether the dynamics of transport were affected, we turned to time-lapse imaging of YFP-GGA1–containing vesicles in control and p56-depleted, live H4 cells. We chose H4 cells for these experiments because they express moderate levels of the transfected constructs and the depletion of p56 is similar to that achieved in HeLa cells (Figure 10, A and B). In previous studies (Puertollano *et al.*, 2003; Polishchuk *et al.*, 2006), we observed the presence of YFP-GGA1 and CD-MPR-CFP on pleiomorphic TCs that bud from the TGN and move toward the peripheral cytoplasm. Some of these TCs were found to be typical clathrin-coated vesicles, whereas others were larger and had a more complex structure (Polishchuk *et al.*, 2006). To increase the time resolution of our analyses, in the present study, we modified the procedure to capture four images per second instead of the previous one image every 3–6 s. Using this modified protocol, we made the surprising observation that, in addition to YFP-GGA1–containing TCs moving from the TGN to the periphery, there was another population of YFP-GGA1–containing TCs that moved in the opposite direction, i.e., from the peripheral cytoplasm to the TGN (Figure 10C and Supplementary Video 1). In control cells, numerous TCs were found to follow long, quasi-linear trajectories in both directions (Figure 10D and Supplementary Video 2). In p56-depleted cells, in contrast, there were fewer mobile TCs and these followed shorter, more convoluted trajectories (Figure 10D and Supplementary Video 2). Quantification of these results showed that depletion of p56 reduced both the number of mobile TCs and the distance traveled by each mobile TC to ~30% of control levels (Figure 10, E and F). These results indicated that p56 controls the dynamics of GGA-containing TCs.

The Ability of p56 To Interact with the GGAs Is Required for its Role in Transport Carrier Dynamics

To determine whether the role of p56 in the regulation of TC mobility depends on its ability to interact with the GGAs, we performed an RNAi rescue assay in live H4 cells. p56 was depleted using an siRNA directed to the 5′ untranslated region of p56. This siRNA was found to be as effective as the siRNA that targeted the coding sequence (Figure 10B). siRNA-treated cells were then rescued with plasmids encoding either a Myc-epitope–tagged, full-length p56 (Myc-p56), or a Myc-epitope–tagged construct lacking the N-terminal,

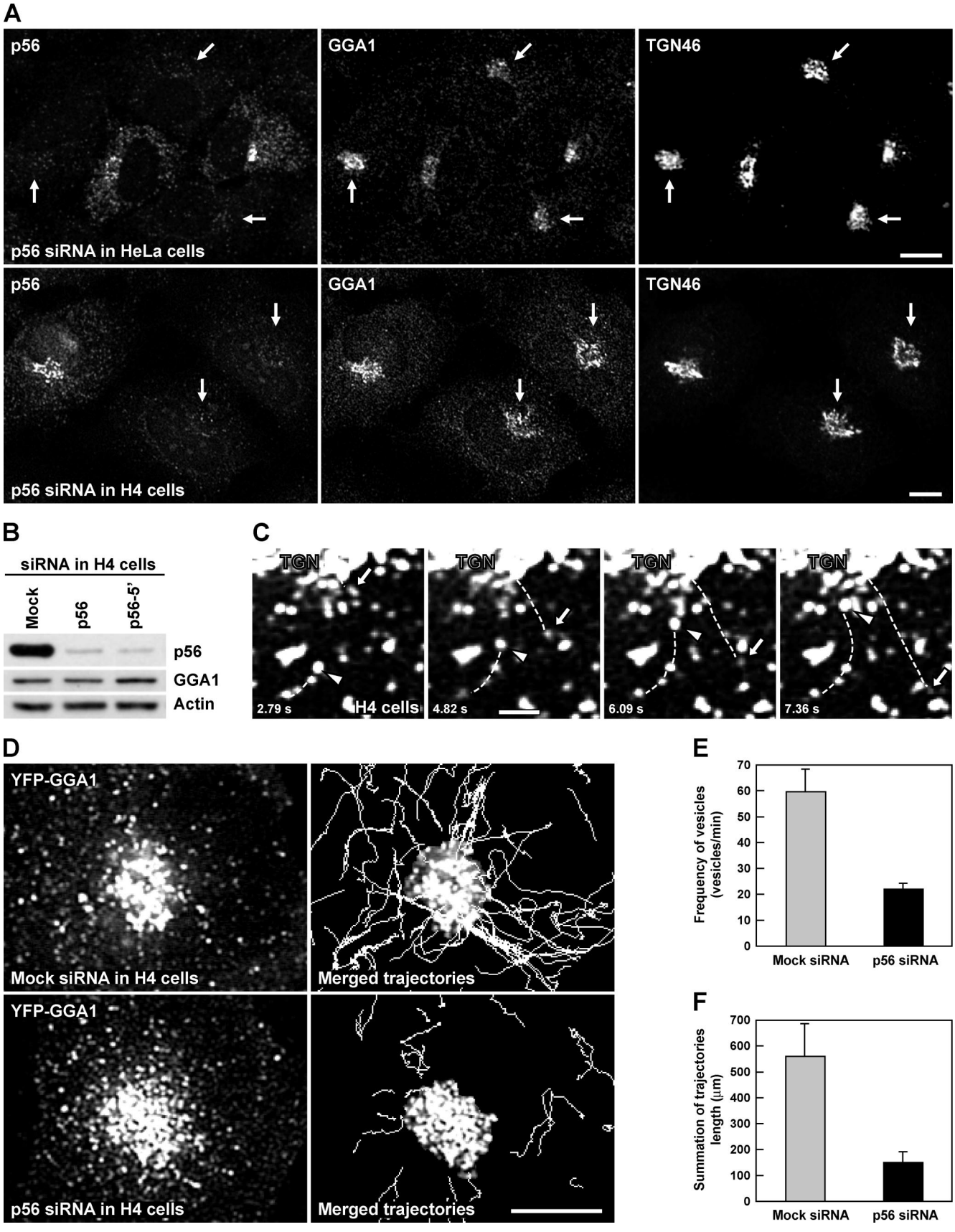

Figure 10. Decreased mobility of YFP-GGA1–containing carriers in cells depleted of p56. (A) HeLa (top row) and H4 cells (bottom row) were transfected twice with siRNAs directed to GAPDH (Mock), or p56. After the second round of transfection, the effects of the RNAi

GGA-interacting segment of p56 (Myc-ΔN-p56; residues 125–441; Collins *et al.*, 2003; Lui *et al.*, 2003). Immunofluorescence microscopy showed that Myc-p56 was correctly targeted to the TGN, where it colocalized with endogenous GGA1, GGA2, and GGA3 (Figure 11A and data not shown). In contrast, Myc-ΔN-p56 was not targeted to the TGN, exhibiting a diffuse cytosolic localization (Figure 11A). Immunoblot analysis showed that expression of Myc-p56 and Myc-ΔN-p56 was indeed resistant to the RNAi treatment (Figure 11B). Expression of Myc-p56 in p56-depleted cells restored the movement of YFP-GGA1–containing TCs in both directions (i.e., from the TGN to the periphery and vice versa; Figure 11, C–E, and Supplementary Video 3), to an extent similar to that observed in mock-treated cells (Figure 10D). Expression of Myc-ΔN-p56 in p56-depleted cells, however, failed to restore TC mobility (Figure 11, C–E, and Supplementary Video 3). These results demonstrated that interaction of p56 with the GGAs is required for its role in the regulation of TC dynamics.

DISCUSSION

Over the past decade it has become established that the main function of the ear domains of clathrin adaptors is to serve as "hubs" for interaction with specific cohorts of accessory proteins. The roles of these accessory proteins are best understood for the more than 20 such proteins that interact with the endocytic AP2 adaptor and that function as regulators, mechanical/assembly factors, and/or alternative adaptors (Traub, 2005). Perturbation or depletion of these AP2-interacting accessory proteins results in inhibition of either global or specific endocytic events. The TGN/endosomal clathrin adaptors, GGAs and AP1, share structurally related GAE domains that interact with a different set of accessory proteins, but the functions of these proteins are much less well understood. Of all the GGA- and AP1-accessory proteins described to date, p56 is unique in that it specifically interacts with the GGAs, and not with AP1, in vivo (Lui *et al.*, 2003; this study). The results of our study now show that p56 functions in close cooperation with the GGAs in the sorting of cathepsin D to lysosomes, probably by promoting the long-range movement of GGA/clathrin-containing TCs through the cytoplasm.

Tight Physical and Biogenetic Relationship of p56 with the GGAs

Some clathrin adaptors and their cognate accessory proteins are expressed in all cells (e.g., AP1A, AP2, AP3A, GAK; Kimura *et al.*, 1997; Boehm and Bonifacino, 2001), whereas others are tissue- or cell-type specific (e.g., AP1B in polarized epithelia, AP3B in the brain, auxilin in the brain; Ahle and Ungewickell, 1990; Boehm and Bonifacino, 2001). The availability of a complete panel of antibodies sensitive enough to detect the endogenous proteins have now allowed us to demonstrate that the three GGAs and p56 belong to the former group, in that they are coexpressed in all cell lines examined (Figure 1). In addition, they all largely colocalize to the TGN and peripheral foci that probably correspond to TCs and endosomes (Figures 2 and 3). Moreover, they physically interact within cells, as demonstrated by FRET (Figure 4A). Finally, overexpression of the GGAs enhances the association of p56 with the TGN (Figure 4B), and RNAi-mediated depletion of any of the GGAs decreases p56 staining at the TGN (Figure 7). Surprisingly, this latter effect is not solely due to decreased recruitment from the cytosol, but to decreased total levels of p56 in the GGA-depleted cells as well (Figure 5). Loss of p56 caused by depletion of one GGA can be suppressed by overexpression of another GGA (Figure 8). These observations indicate that the total levels of the GGAs determine the stability of p56. The relationship between these proteins is thus specific and tight, involving even a biogenetic dependence of p56 on the GGAs. The understanding of this relationship is helpful for the interpretation of the effects of RNAi-mediated depletion of the GGAs, which also decreases levels of p56. The cellular effects of GGA depletion could, therefore, be partly due to decreased p56 levels.

Another interesting finding in our study was that depletion of one GGA did not alter the localization or levels of the other two. The GGAs, therefore, behave as biogenetically independent entities. This finding contrasts with that of a previous study (Ghosh *et al.*, 2003b), in which the depletion of any one GGA decreased the levels of the other two. This was not due to off-target effects of the RNAi, because the levels of the two indirectly affected GGAs could be restored by treatment with proteasomal inhibitors or by transfection with RNAi-resistant cDNA encoding the target GGA (Ghosh *et al.*, 2003b). We do not know the reason for these differences, especially as both studies were carried out with HeLa cells. A possible explanation is the different RNAi methodologies that were used to knock down GGA expression: stable transfection of vectors encoding siRNAs in the previous study (Ghosh *et al.*, 2003b) and transient transfection of synthetic siRNAs in the present study. Our observations indicate that, over a span of 3–5 d of siRNA treatment, the levels of the three GGAs are not interdependent. The three GGAs are not entirely redundant, however, because depletion of any single GGA causes partial reduction of p56 levels (Figure 5) and cathepsin D missorting (Figure 9; Ghosh *et al.*, 2003b). We attribute this to a dosage effect and not to an effect of depleting one GGA on the levels of the other two.

Figure 10 (cont). depletion on the distribution of GGA1 in cells were assessed by indirect immunofluorescence. Mixed mock- and p56-depleted cells grown on coverslips were fixed, permeabilized, and triple-labeled with rabbit antibody to p56, mouse antibody to GGA1, and sheep antibody to TGN46, followed by Alexa-488–conjugated donkey anti-rabbit IgG, Alexa-594–conjugated donkey anti-mouse IgG, and Alexa-647–conjugated donkey anti-sheep IgG. Stained cells were examined by confocal fluorescence microscopy. Arrows indicate the position of the Golgi complex in p56-depleted cells. (B) H4 cells were transfected twice with siRNAs directed to GAPDH (Mock) or either of two siRNAs directed to the coding sequence or the 5′ untranslated region of p56 (p56 and p56-5′). After the second round of transfection, equivalent amounts of siRNA-treated cells were subjected to SDS-PAGE and immunoblotting using antibodies to p56, GGA1, or actin (loading control). (C–F) H4 cells were transfected with siRNAs directed to GAPDH (Mock) or p56 as indicated in A and after the second round of siRNA treatment were transfected with YFP-GGA1. The effects of the RNAi on the mobility of vesicles containing YFP-GGA1 in cells were assessed by time-lapse microscopy. (C) Mock siRNA-treated cell showing a vesicle moving away from the TGN region (trajectory indicated by arrow) and another vesicle moving toward the TGN region (trajectory indicated by arrowhead). Time after the start of imaging (in seconds) is shown in the bottom left of each panel. (D) The first frame acquired for either a mock- or a p56-depleted cell is shown on the left. The pictures on the right were generated by merging images of the TGN region acquired over a ~110-s period; the trajectories of mobile vesicles are shown as lines. The frequency of mobile vesicles (E) and the summation of the length of the trajectories (F) were quantified for mock- and p56-depleted cells. Bars represent the mean ± SD from three independent experiments. Bars, 10 μm (A and D), 2 μm (C).

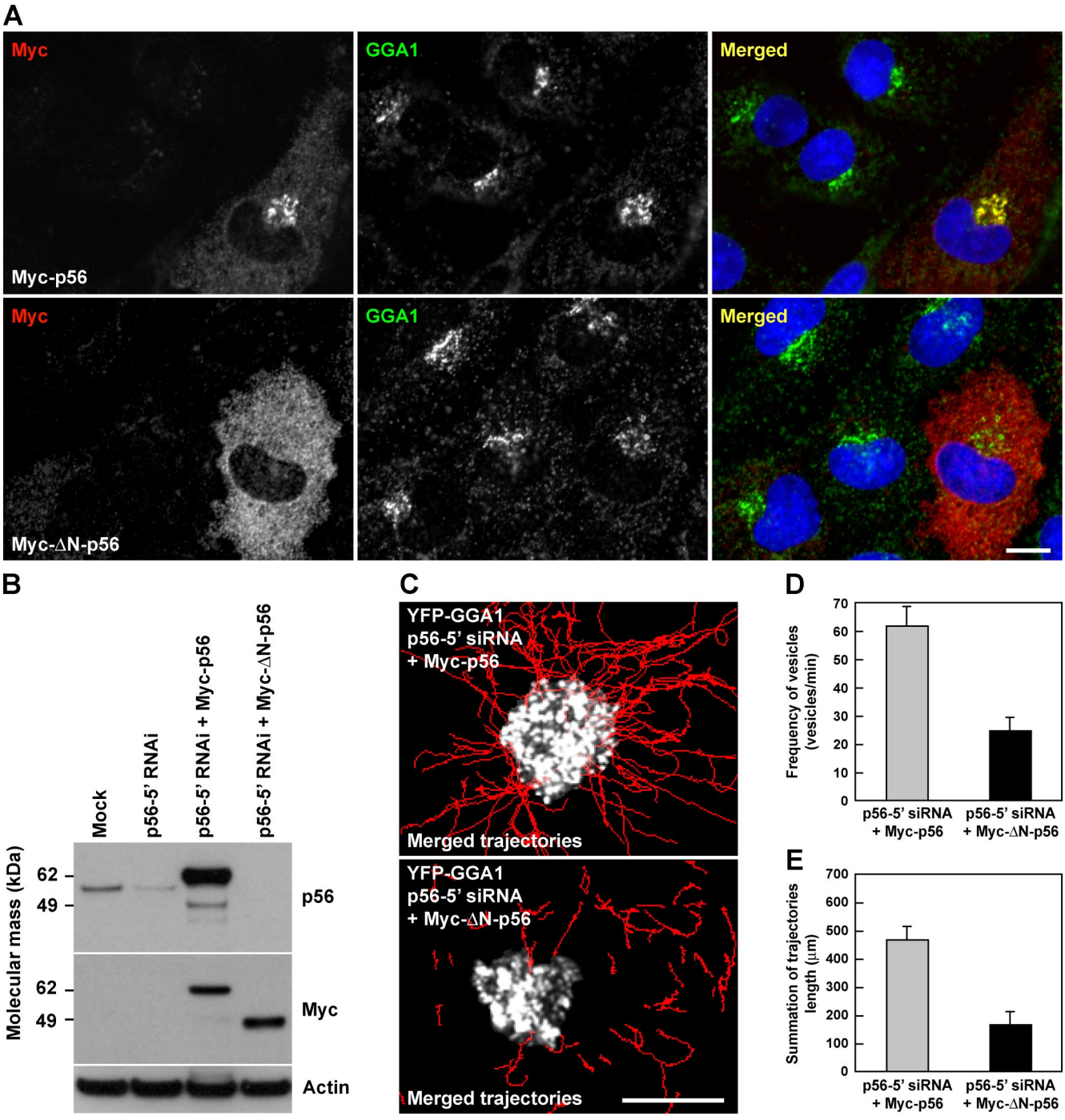

Figure 11. Binding of p56 to GGAs is required for the mobility of YFP-GGA1-containing carriers. (A) NRK cells transfected either with Myc-tagged, full-length p56 (Myc-p56) or a Myc-tagged construct lacking the N-terminal, GGA-interacting segment of p56 (Myc-ΔN-p56; residues 125–441) were fixed, permeabilized, and double-labeled with mAb to the Myc epitope and rabbit polyclonal antibody to GGA1, followed by Alexa-594–conjugated donkey anti-mouse IgG (red channel) and Alexa-488–conjugated donkey anti-rabbit IgG (green channel). Nuclei were stained with Hoechst 33342 dye (blue channel). Stained cells were examined by confocal fluorescence microscopy. Merging red, green, and blue channels generated the third picture; yellow indicates overlapping localization of the green and red channels. (B) H4 cells were transfected twice with siRNA directed to GAPDH (Mock), or with siRNA directed to the 5′ untranslated region of p56 (p56-5′). After the second round of siRNA treatment, p56-depleted cells were transfected either with Myc-p56 or Myc-ΔN-p56, and after 16 h, equivalent amounts of cells were subjected to SDS-PAGE and immunoblotting using antibodies to p56 (raised against an N-terminal peptide), the Myc epitope, or actin (loading control). (C–E) H4 cells were transfected with the p56-5′ siRNA as indicated in B and after the second round of siRNA treatment were cotransfected with YFP-GGA1 and either with Myc-p56 or Myc-ΔN-p56. The effects of the expression of the Myc-epitope-tagged proteins on the mobility of vesicles containing YFP-GGA1 were assessed by time-lapse microscopy. (C) The TGN region of the first frame acquired for p56-depleted cells, expressing either Myc-p56 (top) or Myc-ΔN-p56 (bottom), was merged with the trajectories of mobile vesicles (red lines) acquired over a ~110-s period. The frequency of mobile vesicles (D) and the summation of the length of the trajectories (E) were quantified for p56-depleted cells expressing either Myc-p56 or Myc-ΔN-p56. Bars represent the mean ± SD from three independent experiments. Bars, (A and C) 10 μm.

Requirement of p56 for Sorting of Procathepsin D to Lysosomes

The ability to deplete cells of p56 without altering the levels of the GGAs (Figure 5) allowed us to test the involvement of p56 in the sorting of procathepsin D to lysosomes. We found that depletion of p56 impaired proteolytic processing of procathepsin D to the intermediate and mature forms, as detected by both immunoblotting (Figure 9, A and B) and pulse-chase and immunoprecipitation analyses (Figure 9, C and D). Because procathepsin D processing occurs upon transport to lysosomes, these observations indicate that p56 is involved in protein sorting to lysosomes. In agreement with previous studies (Ghosh *et al.*, 2003b), we also found that depletion of single GGAs caused partial missorting of procathepsin D (Figure 9), but this could be in part due to the decreased levels of p56 caused by GGA depletion (Figure 5). Also of interest is the observation that depletion of clathrin causes a profound inhibition of procathepsin D sorting to lysosomes (Figure 9). This agrees with a previous observation made through the use of antisense RNA targeting the clathrin heavy chain (Iversen *et al.*, 2003) and is in line with the requirement of clathrin adaptors (i.e., GGAs and AP1) for procathepsin D sorting (Figure 9; Meyer *et al.*, 2000; Ghosh *et al.*, 2003b; Hirst *et al.*, 2005). It contrasts, however, with observations made in the chicken B lymphocyte cell line, DT40, in which the accumulation of another acid hydrolase, β-glucuronidase, and the integral membrane protein, LEP100, within lysosomes was unaffected by elimination of the clathrin heavy chain (Wettey *et al.*, 2002). The results from this latter study could stem from the use of a mutant cell line that adapted to the lack of clathrin expression, because all other evidence (Iversen *et al.*, 2003; Janvier and Bonifacino, 2005) points to a critical role for clathrin and some of its adaptors in the sorting of both luminal and transmembrane components of lysosomes.

p56 Regulates the Mobility of GGA-containing Transport Carriers

Despite the impairment of procathepsin D sorting, we did not observe any obvious changes in the distribution of the CI-MPR by immunofluorescence microscopy in p56-depleted cells (data not shown). This could simply reflect the low resolution of this technique to distinguish different juxtanuclear, TGN, or endosomal compartments. Alternatively, p56 depletion could alter the dynamics of transport between the TGN and endosomes, without causing noticeable changes in the overall appearance of CI-MPR–containing structures. This seems, in fact, to be the case as depletion of p56 decreased the mobility of GGA-containing TCs (Figure 10). Previous studies documented the existence of pleiomorphic TCs that contain GGA, AP1, clathrin, CI-MPR, and CD-MPR and move from the TGN toward the peripheral cytoplasm (Huang *et al.*, 2001; Waguri *et al.*, 2002; Puertollano *et al.*, 2003; Polishchuk *et al.*, 2006). These carriers were proposed to mediate the long-range distribution of a pool of MPRs and their cargo hydrolase precursors between the TGN and peripheral endosomes. Improved time resolution allowed us to observe another population of GGA-containing TCs that move from the periphery to the center of the cell. At present we do not know the function of such centripetal TCs. One possibility is that the GGAs have an additional role in retrograde transport, as recently proposed (He *et al.*, 2005). Alternatively, the GGAs may not play any role in retrograde transport but just remain passively associated with retrograde TCs after their forward sorting function is fulfilled. In any event, p56 depletion inhibits the movement of both forward and retrograde TCs (Figure 10), perhaps explaining the unchanged steady-state distribution of MPRs. Because the movement of the forward TCs is dependent on microtubules (Waguri *et al.*, 2002; Puertollano *et al.*, 2003), it is tempting to speculate that p56 could participate in linking GGA-containing carriers to microtubule motors. Precedent for the coupling of a clathrin adaptor with a microtubule motor is the demonstration of an interaction of the β1 subunit of AP1 with the kinesin, KIF13A, which enables movement of CI-MPR–containing vesicles from the TGN to the plasma membrane (Nakagawa *et al.*, 2000). These findings support the notion that the roles of clathrin coats extend beyond cargo selection and vesicle budding.

The Canonical Interaction of p56 with GGAs Is Required for Transport Carrier Mobility

Expression of RNAi-resistant, full-length p56 restored the dynamics of TC movement in p56-depleted cells, thus demonstrating the specificity of the phenotype. However, expression of a p56 variant lacking the N-terminal, GGA-interacting segment failed to restore movement (Figure 11). This demonstrated that this function of p56 is dependent on its interaction with the GGAs. The N-terminal segment of p56 comprises the sequence, FGGF, which binds to the ear domain of the GGAs (Collins *et al.*, 2003). This sequence belongs to a group of sequences shared by GGA- and AP1-accessory proteins that fit certain canonical motifs (Page *et al.*, 1999; Kent *et al.*, 2002; Collins *et al.*, 2003; Duncan *et al.*, 2003; Mattera *et al.*, 2003, 2004; Miller *et al.*, 2003; Mills *et al.*, 2003). These canonical ear-motif interactions have been extensively characterized, both biochemically and structurally. However, their requirement for the function of TGN accessory proteins is poorly understood. Our findings now demonstrate that a canonical interaction between a TGN/endosomal clathrin adaptor and an accessory protein is indeed required for function.

ACKNOWLEDGMENTS

We thank Hsin-I Tsai for expert technical assistance; M. S. Robinson, M. S. Marks, T. A. Rouault, C. L. Cadilla, and E. O. Long for kind gifts of reagents; and W. Lindwasser for critical review of the manuscript. The Intramural Research Program of the National Institutes of Health supported this research.

REFERENCES

Ahle, S., and Ungewickell, E. (1990). Auxilin, a newly identified clathrin-associated protein in coated vesicles from bovine brain. J. Cell Biol. *111*, 19–29.

Boehm, M., and Bonifacino, J. S. (2001). Adaptins: the final recount. Mol. Biol. Cell *12*, 2907–2920.

Bolte, S., and Cordelières, F. P. (2006). A guided tour into subcellular colocalization analysis in light microscopy. J. Microsc. *224*, 213–232.

Boman, A. L., Zhang, C. J., Zhu, X., and Kahn, R. A. (2000). A family of ADP-ribosylation factor effectors that can alter membrane transport through the trans-Golgi. Mol. Biol. Cell *11*, 1241–1255.

Bonifacino, J. S. (2004). The GGA proteins: adaptors on the move. Nat. Rev. Mol. Cell Biol. *5*, 23–32.

Bowers, K., and Stevens, T. H. (2005). Protein transport from the late Golgi to the vacuole in the yeast *Saccharomyces cerevisiae*. Biochim. Biophys. Acta *1744*, 438–454.

Burgos, P. V., Klattenhoff, C., de la Fuente, E., Rigotti, A., and González, A. (2004). Cholesterol depletion induces PKA-mediated basolateral-to-apical transcytosis of the scavenger receptor class B type I in MDCK cells. Proc. Natl. Acad. Sci. USA *101*, 3845–3850.

Collins, B. M., Praefcke, G. J., Robinson, M. S., and Owen, D. J. (2003). Structural basis for binding of accessory proteins by the appendage domain of GGAs. Nat. Struct. Biol. *10*, 607–613.

Dell'Angelica, E. C., Puertollano, R., Mullins, C., Aguilar, R. C., Vargas, J. D., Hartnell, L. M., and Bonifacino, J. S. (2000). GGAs: a family of ADP ribosylation factor-binding proteins related to adaptors and associated with the Golgi complex. J. Cell Biol. *149*, 81–94.

Doray, B., Ghosh, P., Griffith, J., Geuze, H. J., and Kornfeld, S. (2002). Cooperation of GGAs and AP-1 in packaging MPRs at the trans-Golgi network. Science *297*, 1700–1703.

Doray, B., and Kornfeld, S. (2001). Gamma subunit of the AP-1 adaptor complex binds clathrin: implications for cooperative binding in coated vesicle assembly. Mol. Biol. Cell *12*, 1925–1935.

Duncan, M. C., Costaguta, G., and Payne, G. S. (2003). Yeast epsin-related proteins required for Golgi-endosome traffic define a gamma-adaptin ear-binding motif. Nat. Cell Biol. *5*, 77–81.

Galperin, E., and Sorkin, A. (2003). Visualization of Rab5 activity in living cells by FRET microscopy and influence of plasma-membrane-targeted Rab5 on clathrin-dependent endocytosis. J. Cell Sci. *116*, 4799–4810.

Ghosh, P., Dahms, N. M., and Kornfeld, S. (2003a). Mannose 6-phosphate receptors: new twists in the tale. Nat. Rev. Mol. Cell Biol. *4*, 202–212.

Ghosh, P., Griffith, J., Geuze, H. J., and Kornfeld, S. (2003b). Mammalian GGAs act together to sort mannose 6-phosphate receptors. J. Cell Biol. *163*, 755–766.

Ghosh, P., and Kornfeld, S. (2004). The GGA proteins: key players in protein sorting at the trans-Golgi network. Eur. J. Cell Biol. *83*, 257–262.

Gordon, G. W., Berry, G., Liang, X. H., Levine, B., and Herman, B. (1998). Quantitative fluorescence resonance energy transfer measurements using fluorescence microscopy. Biophys. J. *74*, 2702–2713.

He, X., Li, F., Chang, W. P., and Tang, J. (2005). GGA proteins mediate the recycling pathway of memapsin 2 (BACE). J. Biol. Chem. *280*, 11696–11703.

Hirst, J., Borner, G. H., Harbour, M., and Robinson, M. S. (2005). The aftiphilin/p200/gamma-synergin complex. Mol. Biol. Cell *16*, 2554–2565.

Hirst, J., Lui, W. W., Bright, N. A., Totty, N., Seaman, M. N., and Robinson, M. S. (2000). A family of proteins with gamma-adaptin and VHS domains that facilitate trafficking between the trans-Golgi network and the vacuole/lysosome. J. Cell Biol. *149*, 67–80.

Hirst, J., Motley, A., Harasaki, K., Peak Chew, S. Y., and Robinson, M. S. (2003). EpsinR: an ENTH domain-containing Protein that Interacts with AP-1. Mol. Biol. Cell *14*, 625–641.

Höning, S., Sosa, M., Hille-Rehfeld, A., and von Figura, K. (1997). The 46-kDa mannose 6-phosphate receptor contains multiple binding sites for clathrin adaptors. J. Biol. Chem. *272*, 19884–19890.

Huang, F., Nesterov, A., Carter, R. E., and Sorkin, A. (2001). Trafficking of yellow-fluorescent-protein-tagged mu1 subunit of clathrin adaptor AP-1 complex in living cells. Traffic *2*, 345–357.

Iversen, T. G., Skretting, G., van Deurs, B., and Sandvig, K. (2003). Clathrin-coated pits with long, dynamin-wrapped necks upon expression of a clathrin antisense RNA. Proc. Natl. Acad. Sci. USA *100*, 5175–5180.

Janvier, K., and Bonifacino, J. S. (2005). Role of the endocytic machinery in the sorting of lysosome-associated membrane proteins. Mol. Biol. Cell *16*, 4231–4242.

Kametaka, S., Moriyama, K., Burgos, P. V., Eisenberg, E., Greene, L. E., Mattera, R., and Bonifacino, J. S. (2007). Canonical interaction of cyclin G-associated kinase with adaptor protein 1 regulates lysosomal enzyme sorting. Mol. Biol. Cell *18*, 2991–3001.

Kalthoff, C., Groos, S., Kohl, R., Mahrhold, S., and Ungewickell, E. J. (2002). Clint: a novel clathrin-binding ENTH-domain protein at the Golgi. Mol. Biol. Cell *13*, 4060–4073.

Kent, H. M., McMahon, H. T., Evans, P. R., Benmerah, A., and Owen, D. J. (2002). Gamma-adaptin appendage domain: structure and binding site for Eps15 and gamma-synergin. Structure (Camb.) *10*, 1139–1148.

Kornfeld, S. (1992). Structure and function of the mannose 6-phosphate/insulinlike growth factor II receptors. Annu. Rev. Biochem. *61*, 307–330.

Koster, A., Saftig, P., Matzner, U., von Figura, K., Peters, C., and Pohlmann, R. (1993). Targeted disruption of the M(r) 46,000 mannose 6-phosphate receptor gene in mice results in misrouting of lysosomal proteins. EMBO J. *12*, 5219–5223.

Kimura, S. H., Tsuruga, H., Yabuta, N., Endo, Y., and Nojima, H. (1997). Structure, expression, and chromosomal localization of human GAK. Genomics *44*, 179–187.

Klumperman, J., Hille, A., Veenendaal, T., Oorschot, V., Stoorvogel, W., von Figura, K., and Geuze, H. J. (1993). Differences in the endosomal distributions of the two mannose 6-phosphate receptors. J. Cell Biol. *121*, 997–1010.

Le Borgne, R., and Hoflack, B. (1997). Mannose 6-phosphate receptors regulate the formation of clathrin-coated vesicles in the TGN. J. Cell Biol. *137*, 335–345.

Ludwig, T., Ovitt, C. E., Bauer, U., Hollinshead, M., Remmler, J., Lobel, P., Ruther, U., and Hoflack, B. (1993). Targeted disruption of the mouse cation-dependent mannose 6-phosphate receptor results in partial missorting of multiple lysosomal enzymes. EMBO J. *12*, 5225–5235.

Ludwig, T., Eggenschwiler, J., Fisher, P., D'Ercole, A. J., Davenport, M. L., and Efstratiadis, A. (1996). Mouse mutants lacking the type 2 IGF receptor (IGF2R) are rescued from perinatal lethality in Igf2 and Igf1r null backgrounds. Dev. Biol. *177*, 517–535.

Lui, W. W., Collins, B. M., Hirst, J., Motley, A., Millar, C., Schu, P., Owen, D. J., and Robinson, M. S. (2003). Binding partners for the COOH-terminal appendage domains of the GGAs and γ-adaptin. Mol. Biol. Cell *14*, 2385–2398.

Manders, E., Stap, J., Brakenhoff, G., van Driel, R., and Aten, J. (1992). Dynamics of three-dimensional replication patterns during the S-phase, analysed by double labelling of DNA and confocal microscopy. J. Cell Sci. *103*, 857–862.

Mardones, G. A., Snyder, C. M., and Howell, K. E. (2006). cis-Golgi matrix proteins move directly to endoplasmic reticulum exit sites by association with tubules. Mol. Biol. Cell *17*, 525–538.

Martina, J. A., Moriyama, K., and Bonifacino, J. S. (2003). BLOC-3, a protein complex containing the Hermansky-Pudlak syndrome gene products HPS1 and HPS4. J. Biol. Chem. *278*, 29376–29384.

Mattera, R., Arighi, C. N., Lodge, R., Zerial, M., and Bonifacino, J. S. (2003). Divalent interaction of the GGAs with the Rabaptin-5-Rabex-5 complex. EMBO J. *22*, 78–88.

Mattera, R., Ritter, B., Sidhu, S. S., McPherson, P. S., and Bonifacino, J. S. (2004). Definition of the consensus motif recognized by gamma-adaptin ear domains. J. Biol. Chem. *279*, 8018–8028.

Meyer, C., Zizioli, D., Lausmann, S., Eskelinen, E. L., Hamann, J., Saftig, P., von Figura, K., and Schu, P. (2000). mu1A-adaptin-deficient mice: lethality, loss of AP-1 binding and rerouting of mannose 6-phosphate receptors. EMBO J. *19*, 2193–2203.

Miller, G. J., Mattera, R., Bonifacino, J. S., and Hurley, J. H. (2003). Recognition of accessory protein motifs by the gamma-adaptin ear domain of GGA3. Nat. Struct. Biol. *10*, 599–606.

Mills, I. G., Praefcke, G. J., Vallis, Y., Peter, B. J., Olesen, L. E., Gallop, J. L., Butler, P. J., Evans, P. R., and McMahon, H. T. (2003). EpsinR: an AP1/clathrin interacting protein involved in vesicle trafficking. J. Cell Biol. *160*, 213–222.

Mullins, C., and Bonifacino, J. S. (2001). The molecular machinery for lysosome biogenesis. Bioessays *23*, 333–343.

Nakagawa, T., Setou, M., Seog, D., Ogasawara, K., Dohmae, N., Takio, K., and Hirokawa, N. (2000). A novel motor, KIF13A, transports mannose-6-phosphate receptor to plasma membrane through direct interaction with AP-1 complex. Cell *103*, 569–581.

Neubrand, V. E., Will, R. D., Mobius, W., Poustka, A., Wiemann, S., Schu, P., Dotti, C. G., Pepperkok, R., and Simpson, J. C. (2005). Gamma-BAR, a novel AP-1-interacting protein involved in post-Golgi trafficking. EMBO J. *24*, 1122–1133.

Nogi, T. *et al.* (2002). Structural basis for the accessory protein recruitment by the gamma-adaptin ear domain. Nat. Struct. Biol. *9*, 527–531.

Owen, D. J., Collins, B. M., and Evans, P. R. (2004). Adaptors for clathrin coats: structure and function. Annu. Rev. Cell Dev. Biol. *20*, 153–191.

Page, L. J., Sowerby, P. J., Lui, W. W., and Robinson, M. S. (1999). Gamma-synergin: an EH domain-containing protein that interacts with gamma-adaptin. J. Cell Biol. *146*, 993–1004.

Polishchuk, R. S., San Pietro, E., Di Pentima, A., Tete, S., and Bonifacino, J. S. (2006). Ultrastructure of long-range transport carriers moving from the trans Golgi network to peripheral endosomes. Traffic *7*, 1092–1103.

Poussu, A., Lohi, O., and Lehto, V. P. (2000). Vear, a novel Golgi-associated protein with VHS and gamma-adaptin "ear" domains. J. Biol. Chem. *275*, 7176–7183.

Puertollano, R., Aguilar, R. C., Gorshkova, I., Crouch, R. J., and Bonifacino, J. S. (2001). Sorting of mannose 6-phosphate receptors mediated by the GGAs. Science *292*, 1712–1716.

Puertollano, R., and Bonifacino, J. S. (2004). Interactions of GGA3 with the ubiquitin sorting machinery. Nat. Cell Biol. *6*, 244–251.

Puertollano, R., van der Wel, N. N., Greene, L. E., Eisenberg, E., Peters, P. J., and Bonifacino, J. S. (2003). Morphology and dynamics of clathrin/GGA1-coated carriers budding from the trans-Golgi network. Mol. Biol. Cell *14*, 1545–1557.

Rasband, W. S. (1997–2007). ImageJ. Bethesda, MD: US National Institutes of Health. USA http://rsb.info.nih.gov/ij/.

Ritter, B., Philie, J., Girard, M., Tung, E. C., Blondeau, F., and McPherson, P. S. (2003). Identification of a family of endocytic proteins that define a new alpha-adaptin ear-binding motif. EMBO Rep. *4*, 1089–1095.

Rizzo, M. A., Springer, G. H., Granada, B., and Piston, D. W. (2004). An improved cyan fluorescent protein variant useful for FRET. Nat. Biotechnol. *22*, 445–449.

Robinson, M. S. (2004). Adaptable adaptors for coated vesicles. Trends Cell Biol. *14*, 167–174.

Shiba, Y., Takatsu, H., Shin, H. W., and Nakayama, K. (2002). Gamma-adaptin interacts directly with Rabaptin-5 through its ear domain. J. Biochem. (Tokyo) *131*, 327–336.

Takatsu, H., Katoh, Y., Shiba, Y., and Nakayama, K. (2001). Golgi-localizing, gamma-adaptin ear homology domain, ADP-ribosylation factor-binding (GGA) proteins interact with acidic dileucine sequences within the cytoplasmic domains of sorting receptors through their Vps27p/Hrs/STAM (VHS) domains. J. Biol. Chem. *276*, 28541–28545.

Takatsu, H., Yoshino, K., and Nakayama, K. (2000). Adaptor gamma ear homology domain conserved in gamma-adaptin and GGA proteins that interact with gamma-synergin. Biochem. Biophys. Res. Commun. *271*, 719–725.

Thompson, J. D., Higgins, D. G., and Gibson, T. J. (1994). CLUSTAL W: improving the sensitivity of progressive multiple sequence alignment through sequence weighting, position-specific gap penalties and weight matrix choice. Nucleic Acids Res. *22*, 4673–4680.

Traub, L. M. (2005). Common principles in clathrin-mediated sorting at the Golgi and the plasma membrane. Biochim. Biophys. Acta *1744*, 415–437.

Waguri, S., Dewitte, F., Le Borgne, R., Rouillé, Y., Uchiyama, Y., Dubremetz, J. F., and Hoflack, B. (2002). Visualization of TGN to endosomes trafficking through fluorescently labeled MPR and AP-1 in living cells. Mol. Biol. Cell *14*, 142–155.

Wahle, T., Prager, K., Raffler, N., Haass, C., Famulok, M., and Walter, J. (2005). GGA proteins regulate retrograde transport of BACE1 from endosomes to the trans-Golgi network. Mol. Cell. Neurosci. *29*, 453–461.

Wasiak, S., Legendre-Guillemin, V., Puertollano, R., Blondeau, F., Girard, M., de Heuvel, E., Boismenu, D., Bell, A. W., Bonifacino, J. S., and McPherson, P. S. (2002). Enthoprotin: a novel clathrin-associated protein identified through subcellular proteomics. J. Cell Biol. *158*, 855–862.

Wettey, F. R., Hawkins, S. F., Stewart, A., Luzio, J. P., Howard, J. C., and Jackson, A. P. (2002). Controlled elimination of clathrin heavy-chain expression in DT40 lymphocytes. Science *297*, 1521–1525.

Wu, X., Zhao, X., Puertollano, R., Bonifacino, J. S., Eisenberg, E., and Greene, L. E. (2003). Adaptor and clathrin exchange at the plasma membrane and trans-Golgi network. Mol. Biol. Cell *14*, 516–528.

Zhu, Y., Doray, B., Poussu, A., Lehto, V. P., and Kornfeld, S. (2001). Binding of GGA2 to the lysosomal enzyme sorting motif of the mannose 6- phosphate receptor. Science *292*, 1716–1718.

Zola, H., and Brooks, D. A. (1981). Techniques for production and characterization of monoclonal hybridoma antibodies. In: Monoclonal Hybridoma Antibodies: Techniques and Applications, ed. J.G.R. Hurrell, Boca Raton, FL: CRC Press, 1–57.